

Embryonic Exposure to VPA Influences Chick Vocalisations: A Computational Study

Antonella M. C. Torrisi¹, Inês Nolasco¹, Paola Sgadò^{*2}, Elisabetta Versace^{*3}, and Emmanouil Benetos^{*1}

¹Centre for Digital Music, Queen Mary University of London, London, UK

²Centre for Mind/Brain Sciences, University of Trento, Rovereto, Italy

³School of Biological and Behavioural Sciences, Centre for Brain and Behaviour, Queen Mary University of London, London, UK

Abstract

In young animals like poultry chicks (*Gallus gallus*), vocalisations convey information about affective and behavioural states. Traditional approaches to vocalisation analysis, relying on manual annotation and predefined categories, introduce biases, limit scalability, and fail to capture the full complexity of vocal repertoires. We introduce a computational framework for automated detection, acoustic feature extraction, and unsupervised learning of chick vocalisations. Applying this framework to a dataset of newly hatched chicks, we identified two primary vocal clusters. We then tested our computational framework on an independent dataset of chicks exposed during embryonic development to vehicle or Valproic Acid (VPA), a compound that disrupts neural development and is linked to autistic-like symptoms. Clustering analysis on the experimental dataset confirmed two primary vocal clusters and revealed systematic differences between groups. VPA-exposed chicks showed an altered repertoire, with a relative increase in softer calls. VPA differentially affected call clusters, modulating temporal, frequency, and energy domain features. Overall, VPA-exposed chicks produced vocalisations with shorter duration, reduced pitch variability, and modified energy profiles, with the strongest alterations observed in louder calls. This study provides a computational framework for analysing animal vocalisations, advancing knowledge of early-life communication in typical and atypical vocal development.

Keywords: bioacoustics, unsupervised learning, chick vocalisation, Valproic Acid, neurodevelopmental model, signal processing

1 Background

From the early stages of life, vocalisations play a crucial role as communicative signals that facilitate social interactions [1], convey affective states [2] and mediate behavioural outcomes [3].

*Authors for correspondence: Paola Sgadò (paola.sgado@unitn.it), Elisabetta Versace (e.versace@qmul.ac.uk), Emmanouil Benetos (e.benetos@qmul.ac.uk)

In young poultry chicks (*Gallus gallus*), vocalisations are an indicator of psychophysiological states [4], welfare conditions [5] and developmental health [6]. Therefore, quantitative analysis of vocalisations is important to support scientific and practical applications.

Chickens have a pivotal socioeconomic value in industrial farming [7, 8]. They are a model in neuroscience for early socio-cognitive abilities [9, 10, 11], in typical and atypical development from the early stages of life [12, 13, 14]. Given the importance of vocalisations, we developed automated methods for detecting and analysing chick vocalisations using an initial dataset of untreated newly-hatched chicks, and applied this approach to an independent dataset that investigated typical and atypical early development.

Although chicken vocalisations have been studied for decades [15, 16], systematic and large-scale approaches for detection and classification have emerged more recently [17]. Historically, classification [15] relied on manual annotation and predefined categories based on visual inspection of spectrograms [18]. This qualitative approach suffers from subjective biases, such as categorising calls based on anthropocentric interpretations, which may overlook biologically relevant aspects of the signal. Recent attempts using supervised methods, such as convolutional neural networks, have made progress, but still encounter limitations, with many calls remaining undefined [17].

Furthermore, despite efforts to characterise vocalisations through acoustic features [16, 19, 20], these analyses have been constrained by reliance on *a priori* call categories rather than empirically defining vocal repertoires through data-driven methods, hindering the development of reproducible classification systems that transcend human biases [21, 20].

To address these issues, we developed a computational framework that integrates automated call detection, multi-feature acoustic analysis, and unsupervised learning to capture variations in the vocal repertoire of young chicks independent of human labels. This approach improves existing classifications via a generalisable, data-driven methodology and establishes a scalable framework for vocalisation analysis.

1.1 Computational frameworks for animal vocalisation analysis

Traditional bioacoustic research, including call detection, feature extraction, and classification, has been constrained by labour-intensive manual processes that are difficult to scale and prone to subjective biases [22]. Computational approaches have begun addressing these limitations [23, 24].

Attention-based architectures and large language models for multi-species recognition tasks have improved the automatic detection and classification of animal vocalisations, by learning context-aware representations and capturing complex acoustic dependencies [25, 26]. However, reliance on supervised learning pipelines based on human-labelled data [27] still imposes an annotation burden and is prone to experimenter biases.

Alternative approaches, such as semi-supervised and few-shot learning methods [28, 29], are less dependent on large labelled datasets, but remain constrained by observer-dependent reference selection, which may limit the representation of acoustic variability. Recent hybrid approaches combine supervised recognition with clustering of residual audio [30], but remain limited by interval-level detection and speech-pretrained embeddings that may not capture avian-specific vocal patterns. Self-supervised methods learn representations directly from unlabelled inputs [31], yet they still require labelled examples for downstream evaluation and thus impose data structure assumptions that may mask the intrinsic vocal repertoires [32, 33].

In contrast, fully unsupervised approaches offer a more data-driven avenue to study natural acoustic categories, free from pre-imposed labels [21]. These methods identify the underlying structure solely on the basis of the inherent statistical properties of the vocal data. This enables the discovery of biologically meaningful structures beyond the limits of human perception [34]. Fine-grained acoustic characterisation can complement these methods through the extraction of one-dimensional features via signal processing techniques [35]. The analysis of features enables a nuanced representation of vocal categories while improving interpretability [36]. While deep learning approaches can capture complex acoustic relationships [37], simpler feature analysis can enhance interpretability, where understanding underlying mechanisms is as important as classification accuracy [32]. This fine-grained approach can capture subtle acoustic distinctions that reflect internal states [3] not readily perceived by humans. Building on these principles, we used a multifaceted computational framework that maps the vocal repertoire of young chicks by combining automatic call detection, acoustic feature analysis and clustering of individual calls based on 20 acoustic features extracted from the temporal, frequency, and energy domains.

1.2 Application to a Valproic Acid model of neurodevelopmental disorders

We tested the generalisability of our computational framework developed on a sample of untreated chicks in the first day after hatching, applying it to a dataset collected to study the effect of embryonic exposure to Valproic Acid (VPA) on early social behaviour [38]. VPA is an anticonvulsant and mood stabiliser for treating epilepsy, migraine, and bipolar disorder [39].

Exposure to this substance during prenatal life interferes with the development of the social brain and increases the risk of developing autism [40]. In animal models, embryonic exposure to VPA leads to deficits associated with autistic-like symptoms, including social deficits, repetitive behaviours and alterations in sensory processing [41, 42].

Several studies have been conducted with rodent models of Autism Spectrum Disorder (ASD) [43] and chicks [44, 45, 14] exposed to VPA during the embryonic phase. In chicks, embryonic exposure to VPA leads to deficits in social behaviour [45, 46], including loss of early social predispositions [38, 47], and compromised aggregative behaviour [45, 44]. Interestingly, the neurobiological bases of some of these deficits are starting to be investigated [48].

Research across species has revealed VPA-related vocal alterations. In marmosets, VPA exposure alters call type distributions [49] and disrupts kinship-related vocal patterns during parent-infant interactions [50]. However, a critical limitation in these studies is the large proportion of unclassified vocalisations, potentially masking additional group differences.

In rodents, prenatal VPA exposure reduces vocalisation rate and call complexity, with shorter calls, elevated peak frequency, and developmental shifts toward simpler call types, reflecting broad alterations in vocal repertoire [51, 43, 52]. In chicks, VPA exposure can reduce the number of vocalisations in threat-related contexts [46] and lower call frequency and amplitude [44]. However, the fine-grained phonetic and acoustic structure of vocalisations in VPA-exposed chicks remains understudied [12]. A comprehensive, data-driven analysis of acoustic features is essential for identifying vocal biomarkers in translational neurodevelopmental research.

1.3 Research contributions

This study offers two main contributions to bioacoustic and neurodevelopmental research. First, we developed an unsupervised computational framework that addresses current methodological limitations in chicks' vocal analysis by reducing reliance on predefined labels and enhancing scalability and reproducible analyses across experimental contexts. Second, we conducted a systematic study of the impact of prenatal exposure to VPA on chick vocalisations. Our analytical framework systematically compared VPA and vehicle-injected (control) chicks through three main analyses: *(i)* call production, *(ii)* repertoire composition through clustering-based analysis and *(iii)* feature analysis. Our approach can identify vocal biomarkers of neurodevelopmental disruption by leveraging unsupervised learning and signal feature analysis that capture fine-grained acoustic variability.

2 Methods

The methods are organised around two core components (see Figure 1): the computational framework and the analytical framework. The computational framework detects chick vocalisations, extracts acoustic features using signal processing, and identifies call clusters. The analytical framework is built upon the resulting call-level dataset, applying multivariate analyses and linear mixed-effects modelling to quantify differences in vocal production and acoustic features between VPA-exposed chicks and controls.

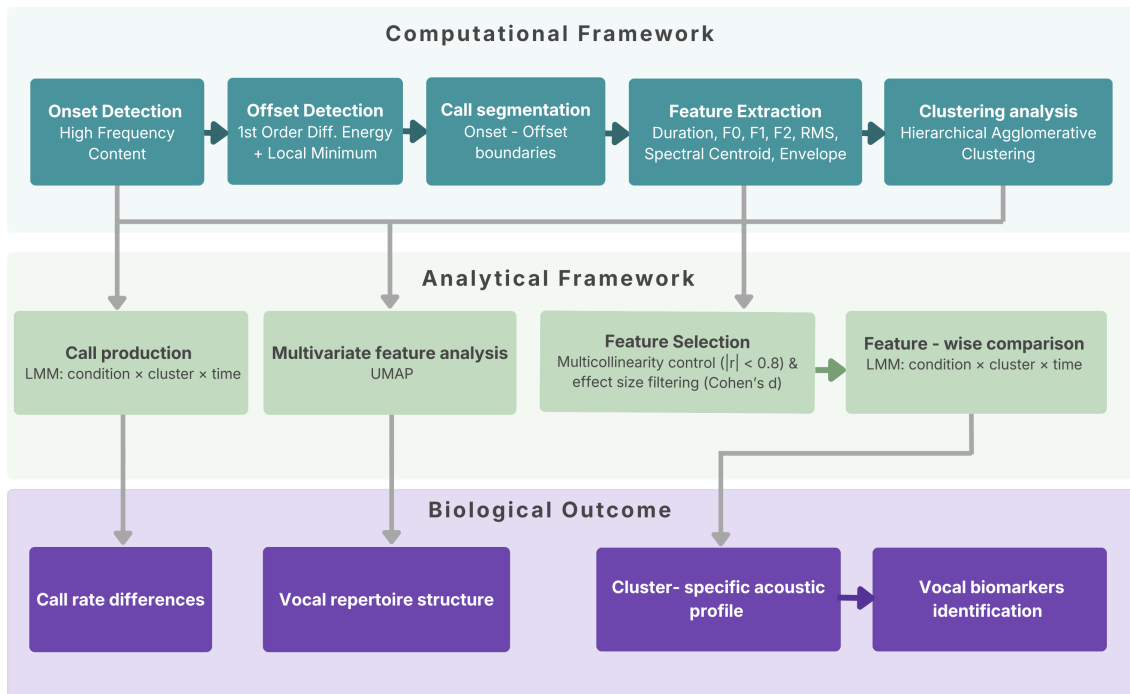


Figure 1: Computational (top), analytical (middle), and biological outcome (bottom) framework for call-level analysis of chick vocalisations. Horizontal arrows indicate processing steps, and vertical arrows information flow across layers.

2.1 Datasets

We used two distinct datasets. We established the computational framework using the development dataset, and then applied it to the experimental dataset, derived from a previous study [38].

2.1.1 Development dataset

This dataset consists of 31 mono-channel audio recordings (WAV format, 44.1 kHz) of visually naïve chicks (18 males, 13 females) tested between 12 and 36 hours after hatching. Each chick was individually recorded for ~10 minutes during free exploration in a rectangular wooden arena (90×60 cm). Each audio recording was extracted from a video acquired through a Microsoft LifeCam, which is a consumer-grade webcam with a built-in microphone rather than specialised acoustic equipment. Vocalisation onsets and offsets were manually annotated by three trained experts using Sonic Visualiser [53], after a training in which they reached an inter-rater reliability of 90%.

For the onset and offset detection task, the development dataset was divided into three subsets, balanced for age and sex: a training set (19 files: 10 males, 9 females; 13,261 calls), a validation set (6 files: 5 males, 3,471 calls), and a testing set (6 files: 4 males, 3,486 calls). The total duration of the analysed recordings was 5 hours and 26 minutes. For feature extraction and clustering analysis, we selected a subset (12 audio files: 7 males; 5,633 calls) with low background noise from the training, validation, and testing datasets.

2.1.2 Experimental dataset

This dataset consists of 46 mono-channel audio recordings (WAV format, 44.1 kHz) of visually-naïve chicks tested within 12 hours after hatching. Each chick was individually recorded for 6 minutes during free exploration in a rectangular wooden arena (85x30 cm). Two objects were projected at the opposite ends of the arena: one object showed changes in speed, while the other maintained a constant speed. The dataset includes a VPA-treated group (27 chicks: 16 males, 14,521 calls) and a control vehicle-injected group (19 chicks: 8 males, 9,028 calls). Audio recordings were extracted from videos acquired through a Microsoft LifeCam. Detailed experimental procedures are described in [38]. Audio recordings were extracted and converted to WAV format (44.1 kHz) using Audacity [54]. Stereo signals were equalised and merged into mono-channel recordings to ensure balanced input contribution. The total duration of the analysed recordings was 4 hours and 18 minutes.

2.2 Computational framework

2.2.1 Pre-processing, onset and offset detection

As an initial step in preprocessing, audio recordings underwent max loudness normalisation to enhance the precision of call detection algorithms and ensure comparability across experiments and sessions. For call onset and offset detection, we used the best algorithms identified in a previous study on the development dataset [55]. For onset detection, we used the High Frequency Content (HFC) algorithm [56], which detects frequency changes within the signal.

For offset detection, we implemented a method based on first-order differencing of the energy signal, followed by local minimum detection within a predefined time window based on the maximum expected

duration of chick calls. Both methods outperformed alternative approaches tested (weighted F1-measure = 0.85 and 0.94, respectively, on the development dataset; see Supplementary Material 4).

To assess the generalisability of the results obtained with our automated approach, we conducted a comprehensive benchmarking evaluation on the annotated experimental dataset. The HFC algorithm achieved an excellent onset detection performance (weighted F1-measure = 0.933, precision = 0.910, recall = 0.961). For the offset detection, the first-order difference method also performed well (weighted F1-measure = 0.885, precision = 0.885, recall = 0.885). Methodological details are reported in the Supplementary Material 4.

2.2.2 Feature extraction

Before feature extraction, a bandpass filter (BPF) was applied to each recording to reduce background noise and focus on the fundamental frequency and first two harmonics of chick vocalisations. The frequency range of the filter was set to 2000-12,600 Hz for the development dataset and to 2000-15,000 Hz for the experimental dataset, to account for range differences. For each segmented call, we extracted different signal components using established methods (for details see Supplementary Material 4): Fundamental Frequency (F0) via PYIN algorithm [57], first and second harmonics (F1, F2) and their magnitudes via FFT [56], Root Mean Square (RMS) [58], Spectral Centroid [56], and signal Envelope via Hilbert transform [59].

From these signal-level features, we characterised each call by calculating 20 one-dimensional statistical descriptors, grouped by domain: temporal (Call Duration, Attack Time, Envelope Slope), frequency (F0 Mean, F0 Standard Deviation, F0 Kurtosis, F0 Skewness, F0 Bandwidth, F0 Slope, F0 1st Order Difference Mean, F0 Mag Mean, F1 Mag Mean, F2 Mag Mean, F0-F1 Mean Ratio, F0-F2 Mean Ratio, Spectral Centroid Mean and Spectral Centroid Standard Deviation, Attack Magnitude), and energy (RMS Mean, RMS Standard Deviation). Detailed feature descriptions and equations to derive them are provided in Table S2. Features were z-score normalised prior to clustering, ensuring they were on a comparable scale for these analyses.

2.2.3 Clustering analysis

For the initial exploratory analysis of chicks' vocal repertoire, we tested hard clustering methods (K-means, Hierarchical Agglomerative Clustering, DBSCAN) and soft clustering methods (Fuzzy C-Means, Gaussian Mixture Models), to capture discrete categories or continuous distributions [36, 60, 34].

To identify the optimal clustering structure for the development dataset, we performed a grid search, testing solutions with 1 to 10 clusters for each algorithm. Three main metrics guided the optimisation: (i) Silhouette Score [34], (ii) Within Cluster Sum of Squares (WCSS) through the Elbow method [34], (iii) Calinski-Harabasz Index (CHI) [34]. For soft clustering methods, we used additional metrics: Fuzzy Partition Coefficient (FPC) [34] for the Fuzzy C-Means, and AIC and BIC [34] for Gaussian Mixture Models. Details of clustering algorithms and performance metrics are described in Supplementary Material 4. For finding the optimal clustering division, the same grid search optimisation approach and evaluation metrics were used for the experimental dataset.

Following quantitative optimisation, we validated clustering results qualitatively by examining calls at varying distances from cluster centroids to assess internal consistency and identify potential outliers. We assessed internal consistency using a percentile-based sampling method: calls within each cluster

were ranked by Euclidean distance from centroids, which represent the mean acoustic profile of each cluster. Given the higher performance of Hierarchical Agglomerative Clustering (HAC) in terms of internal consistency, fewer outliers and interpretability, we report the results of this clustering method. Hierarchical clustering structure for both datasets was visualised through dendograms, where branch height represents the Ward distance at which clusters merge.

2.3 Analytical framework for biological comparisons

To assess whether embryonic VPA exposure alters chick vocalisations, we applied an analytical framework to the output of the computational framework. We progressed from call production analysis to fine-grained acoustic characterisation of vocalisation clusters. To analyse the effect of VPA exposure on the total number of calls, we fitted a Linear Mixed-Effects Model (LMM) with time bin (1-6 minute), experimental condition (control *versus* VPA), call cluster membership, and their interactions as fixed effects. Individual chick identity was included as a random intercept to account for repeated measures. Likelihood ratio tests based on AIC values were used to identify the minimum adequate model via progressive simplifications [61].

To investigate the effect of VPA exposure on acoustic features, we reduced multicollinearity by selecting one feature from each highly correlated pair (Pearson $|r| \geq 0.8$) based on discriminative power (Cohen's d) or biological interpretability (See Supplementary material, Section .1 for details). Each feature was analysed using the same LMM approach described above. We estimated effect sizes using partial eta-squared (η_p^2) and applied False Discovery Rate (FDR) correction to control for multiple testing. To understand whether VPA produced cluster-specific effects, we conducted Tukey-adjusted post hoc comparisons. Results were organised by acoustic domain (temporal, energy, and frequency domains) to facilitate biological interpretation.

3 Results

3.1 Computational results

3.1.1 Clustering results in the Development dataset

HAC identified two optimal clusters in chicks' vocal repertoire (Figure 2A), confirmed by Silhouette at $K = 2$ (0.262) and CHI (1820.717). UMAP visualisation (Figure 2 B) shows that chicks' vocalisations are distributed along a continuum, rather than occupying two distinct embedding spaces.

Qualitative inspection of calls within each cluster revealed distinct acoustic profiles. Cluster 0 comprised soft calls with shorter duration, lower pitch, and lower attack time; cluster 1 comprised calls with higher energy, longer duration, and higher attack time. Spectrograms of representative calls for each cluster are shown in Figure 2 A. Representative calls are derived from the 5th percentile of the Euclidean distance-to-centroid distribution, representing the most central and characteristic vocalisations for each cluster.

3.1.2 Clustering analysis results in experimental dataset (VPA *versus* control)

In the experimental dataset, we applied the HAC method independently to the VPA and control groups. For the VPA-treated group, HAC showed an optimal clustering division at $K = 2$, as indicated by the

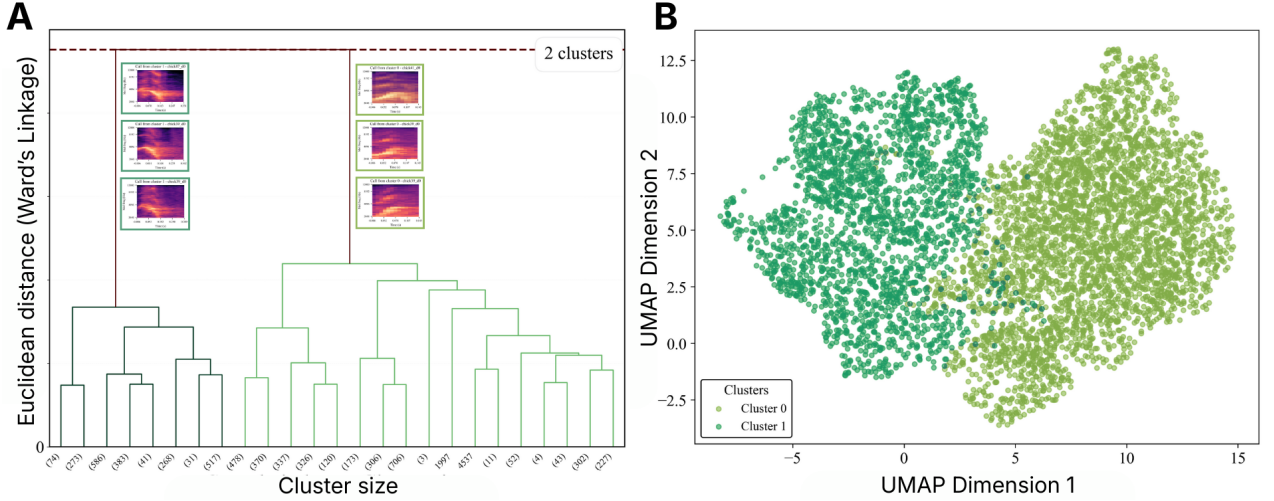


Figure 2: A) Dendrogram of the development dataset showing the clustering structure and optimal cut points, and spectrograms of representative calls extracted from cluster 0 and cluster 1. Within the main clusters, we observed further branching; B) UMAP projection divided into $K = 2$ clusters using HAC.

peak of Silhouette Score (0.425) and CHI (1724.68; See Supplementary FigureS1). The Elbow method applied to the WCSS identified $K = 5$ (WCSS = 206842.54; see Supplementary Figure S2) as optimal division, suggesting a possible substructure in the data. However, the relatively low Silhouette Score at $K = 5$ (0.126) suggested poor cluster separation, and therefore an implausible division.

The dendrogram structure supports the quantitative findings, showing clear branching patterns that align with the $K = 2$ solution (see Figure 3A). UMAP projection at $K = 2$ for VPA-exposed chicks (Figure 3B) shows cluster overlap, and a higher number of calls assigned to cluster 0.

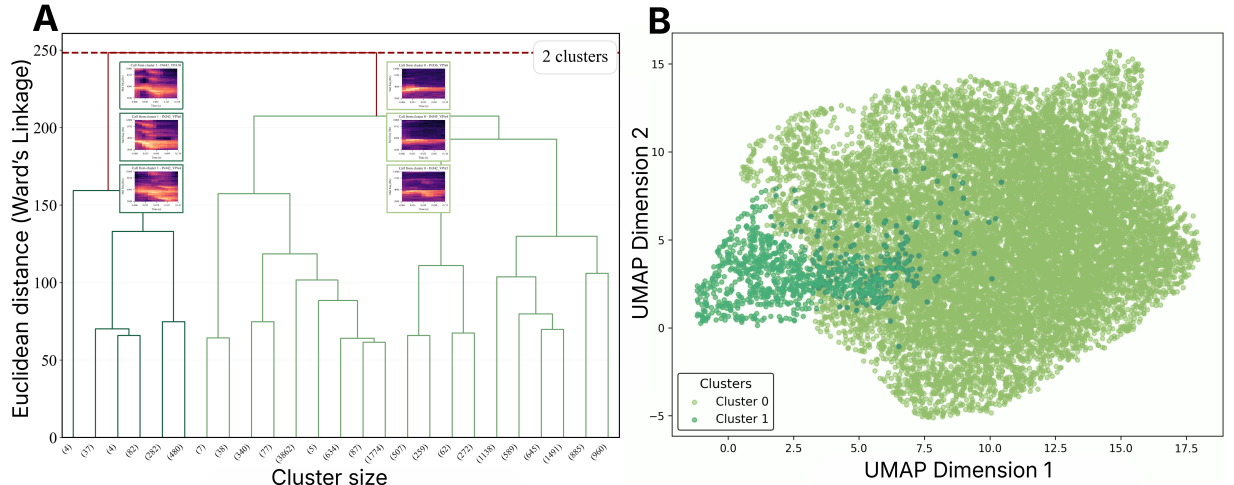


Figure 3: A) Dendrogram for VPA-treated chicks showing the clustering structure and optimal cut points, and spectrograms of representative calls from cluster 0 and cluster 1. Within the main clusters, we observed further branching; B) UMAP projection for VPA-treated chicks with $K = 2$ clusters.

Similarly, the control group showed optimal clustering at $K = 2$ (Silhouette Score: 0.393; CHI: 1820.28), with $K = 3$ (Silhouette Score: 0.347) also providing a reasonable balance between separation and model complexity. As observed in the VPA group, the Elbow method identified $K = 5$ (WCSS = 120806.51) as optimal cluster division. However, the corresponding low Silhouette Score (0.120) indi-

cated significant cluster overlap and implausible divisions for this value. The dendrogram for the control chicks showing the cluster division into 2 groups can be observed in Figure 4A. The UMAP representation (Figure 4B) shows that the control group displayed more clearly delineated clusters compared to the VPA group. A higher number of calls is assigned to cluster 0, especially in the VPA group.

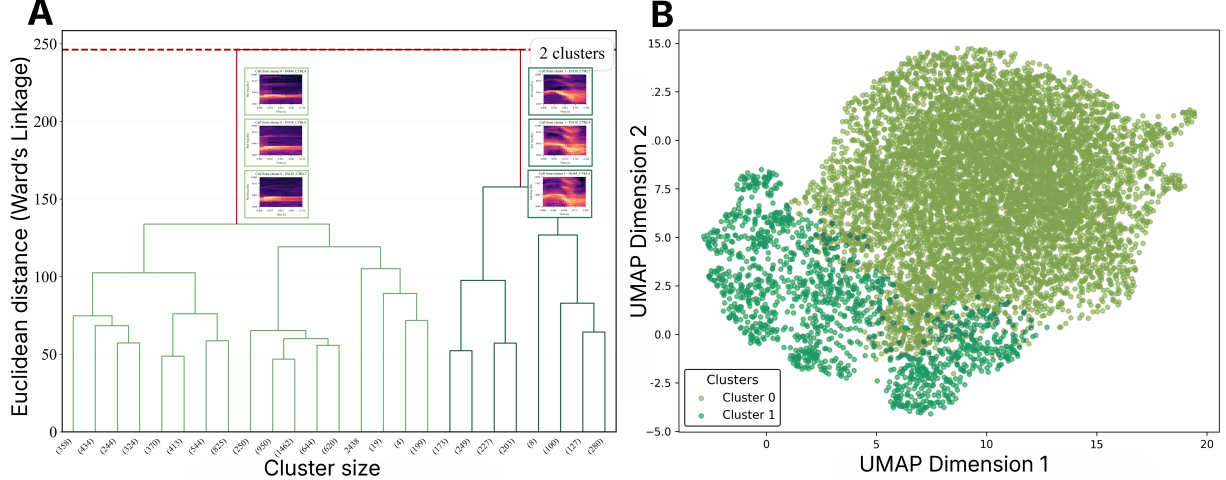


Figure 4: A) Dendrogram for control chicks showing the clustering structure and optimal cut points, and spectrograms of representative calls from cluster 0 and cluster 1. Within the main clusters, we observed further branching; B) UMAP projection for control chicks with $K = 2$ clusters.

Representative calls nearest to cluster centroids are shown in Figures 3A and 4A.

The spectrograms reveal similar patterns across experimental groups. To ensure cluster comparability between groups, we verified correspondence by examining acoustic profiles and representative spectrograms from each group. Qualitatively, calls assigned to cluster 0 in the VPA group closely resemble those in cluster 0 of the control group. Similarly, the calls in cluster 1 of the VPA group are comparable to those in cluster 1 of the control group. Calls in cluster 0 appear shorter in duration, characterised by lower frequency and energy, and lack the second harmonic in both groups. These qualitative observations suggest that the clustering procedure captured consistent vocal categories across experimental groups, with comparable acoustic profiles emerging for analogous clusters. However, subtle variations in temporal, frequency, and energy domain acoustic features may reveal the underlying effects of VPA treatment on vocal production. The quantitative distribution of calls across clusters confirmed these qualitative observations and revealed a pronounced imbalance in both groups. In the control group, 7,661 calls were assigned to cluster 0 and 1,367 to cluster 1. In the VPA group, the imbalance was more pronounced, with 13,632 calls in cluster 0 and only 889 calls in cluster 1.

3.2 Analytical results

3.2.1 Number and Rate of Calls in the Experimental Dataset

The minimum adequate model for the number of calls produced includes Cluster membership ($\chi^2 = 299.34$, $p < 0.001$), Condition ($\chi^2 = 38.78$, $p < 0.001$) and their interaction ($\chi^2 = 33.00$, $p < 0.001$), indicating VPA exposure affects the two call types differently.

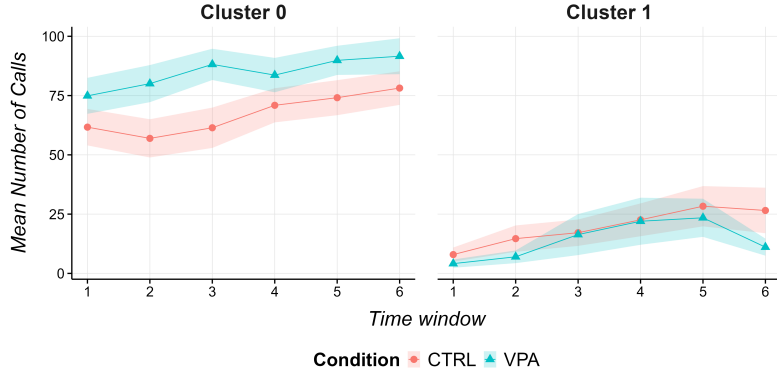


Figure 5: Mean number of calls across 6 time bins by condition and cluster membership. Mean \pm SEM.

Both groups produced significantly more cluster 0 than cluster 1 calls (control: 67.2 vs 13.9 calls per time bin, $p < 0.001$; VPA: 84.4 vs 10.9 calls per time bin, $p < 0.001$). VPA exposure increased cluster 0 calls (+17.2 calls per time bin, $p = 0.006$), whilst producing a trend towards decreased cluster 1 calls (−3.0 calls per time bin, $p = 0.059$).

3.2.2 Feature analysis

After excluding multicollinear features, the analysis included, for the temporal domain: Call Duration and Envelope Slope; for the energy domain: RMS Mean; for the frequency domain: F0 Standard Deviation, F0 Skewness, F0 Kurtosis, F0 1st Order Difference, F0 Slope, F0 Magnitude Mean, F1 Magnitude Mean, F2 Magnitude Mean, F1-F0 Ratio, F2-F0 Ratio, Spectral Centroid Mean, Spectral Centroid Standard Deviation, and Attack Magnitude. Full results are reported in Supplementary TableS4.

Temporal domain features For the Call Duration, the minimum adequate model included the interaction between Condition, Cluster membership and Time bin (see Supplementary Table S4, Figure 6). The same pattern applies to the Envelope Slope (Supplementary Table S4, Figure S7). While for cluster 0 calls we observed no differences between conditions, in cluster 1 calls, the Duration was longer for control chicks compared to VPA chicks, and this difference became stronger over time.

For cluster 0 calls, we observed no differences between conditions, whilst for cluster 1 calls, the Duration was longer for control chicks compared to VPA chicks, and this difference became stronger over time.

Energy features For the RMS mean, the minimum adequate model included the interaction between Condition, Cluster membership and Time bin (see Supplementary Table S4). While cluster 0 calls showed lower RMS mean values in VPA compared to control chicks, cluster 1 calls exhibited the opposite pattern. These condition-dependent differences varied over time, as shown in Figure 7.

Frequency domain features Similar patterns emerged for fundamental frequency variability features (F0 Standard Deviation, F0 Kurtosis, F0 1st Order Difference, F0 Slope, and F0 Skewness), with the minimum adequate model including the interaction between Condition, Cluster membership, and Time bin (Supplementary Table S4):

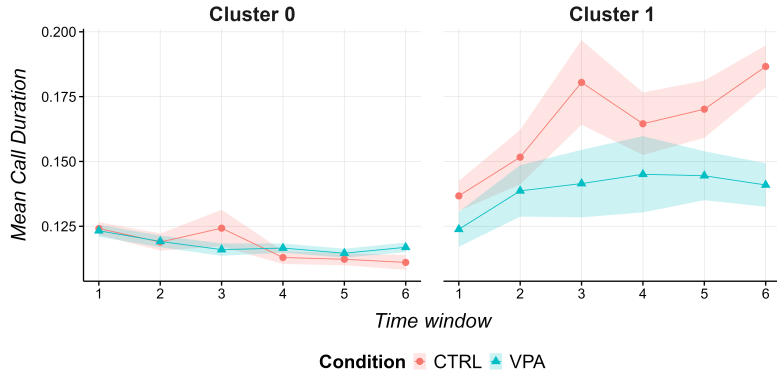


Figure 6: Call Duration across 6 time bins, plotted by condition and cluster (2-cluster solution). Mean \pm SEM.

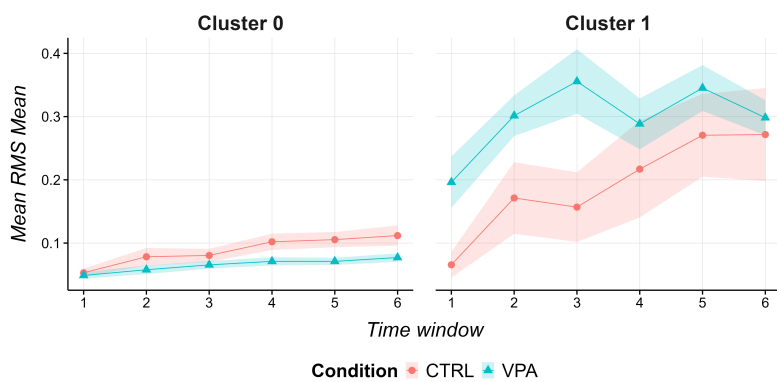


Figure 7: RMS Mean across 6 time bins, plotted by condition and cluster (2-cluster solution). Mean \pm SEM.

For F0 Standard Deviation, VPA exposure reduced F0 variability in cluster 1 calls (Figure 8A), suggesting flattened pitch dynamics over the session, while no significant difference was found for cluster 0 calls between conditions. For F0 Kurtosis, control chicks showed lower F0 kurtosis in cluster 1 versus cluster 0 calls, indicating flatter pitch distribution, while VPA-treated chicks showed reduced cluster differences, making cluster 1 calls more similar to cluster 0 calls in pitch distribution (Figure 8B). For F0 Slope, while cluster 0 calls showed no condition differences, cluster 1 calls had reduced F0 slope values in VPA compared to control chicks. This attenuation was evident in the early temporal bins, effectively diminishing the usual separation in pitch change rate between the two call types (see Figure 8C). Similarly, for the F0 first-order difference, patterns broadly mirrored those observed for the F0 Slope. Cluster 0 calls showed no differences between conditions, while cluster 1 calls exhibited reduced F0 first-order difference variation (narrowing the typical divergence in pitch modulation between clusters) in VPA compared to control chicks. This difference was most pronounced in early time bins (see Figure 8D). For F0 Skewness, we observed similar patterns of interaction. However, effect sizes were smaller than other frequency variability features (Supplementary material .1 and Figure S9). Overall, VPA embryonic exposure fundamentally altered the frequency modulation of cluster 1 calls.

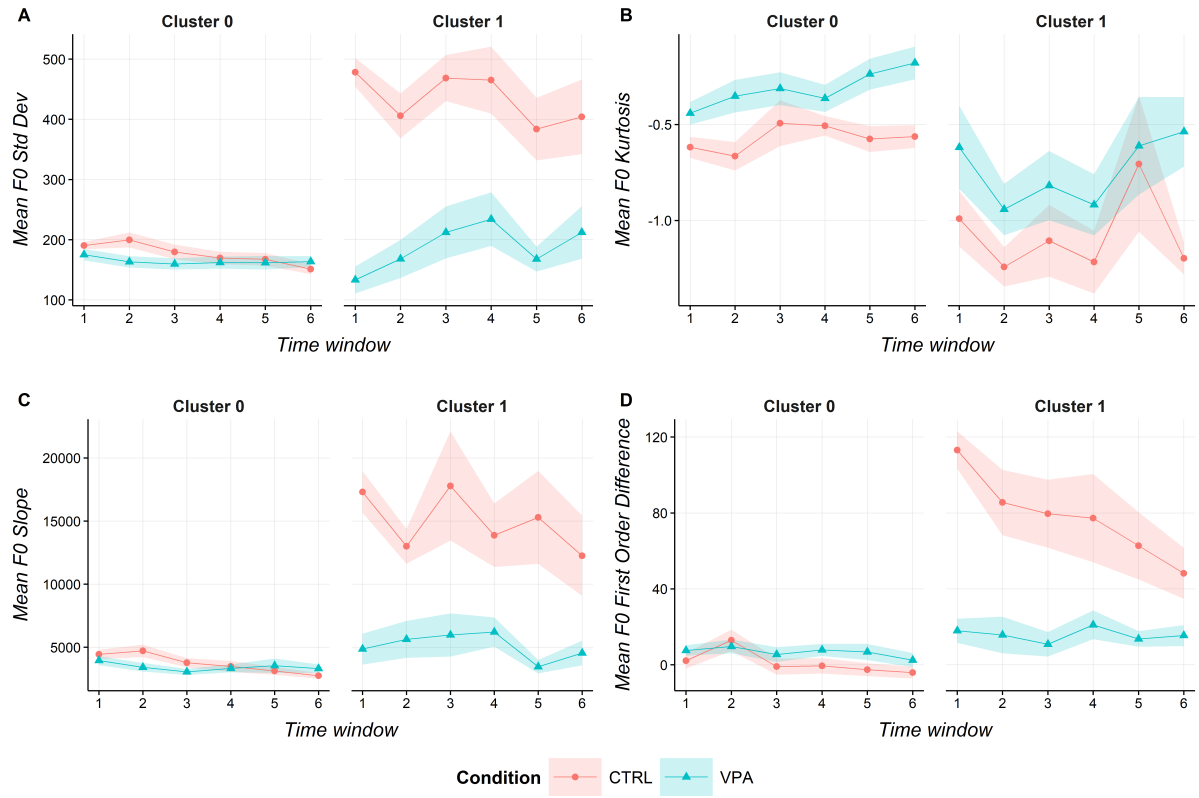


Figure 8: Frequency-domain features across 6 time bins by condition and cluster. (A) F0 Standard Deviation, (B) F0 Kurtosis, (C) F0 Slope, (D) F0 1st Order Difference. Mean \pm SEM.

Spectral features showed strong condition-dependent changes and varied between clusters. For the Spectral Centroid Mean, the minimum adequate model included the interaction between Condition, Cluster membership, and Time bin (see Supplementary Table S4). Cluster 0 calls showed higher spectral centroid values in VPA compared to control chicks across all time bins, while cluster 1 calls exhibited a complex temporal pattern with VPA effects varying relative to controls across the session (see Fig-

ure 9A). For the Spectral Centroid Standard Deviation, the minimum adequate model also included the interaction between Condition, Cluster membership and Time bin (see Supplementary Table S4). Both clusters showed consistently reduced spectral variability under VPA conditions compared to controls, with cluster 1 exhibiting larger decreases than cluster 0, indicating that VPA exposure leads to more stereotyped spectral characteristics for both call types (see Figure 9B).

Finally, for Attack Magnitude, the minimum adequate model included the interaction between Condition, Cluster membership, and Time bin (see Supplementary Table S4). VPA-exposed chicks showed slightly lower attack magnitude values for cluster 0 calls, but higher values for cluster 1 calls compared to control chicks across time bins. Notably, while control chicks demonstrated progressive increases in attack magnitude across the recording session, VPA-exposed chicks maintained consistently high values with reduced temporal variability (see Figure 9C).

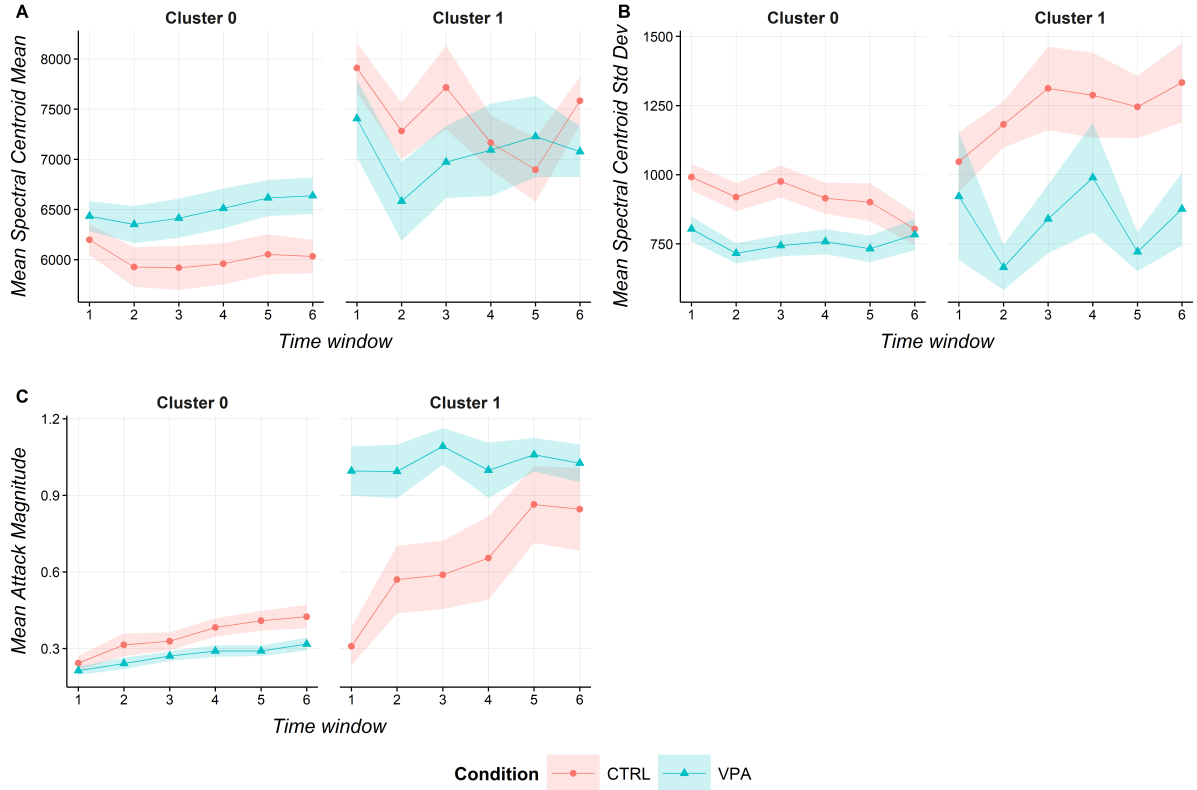


Figure 9: Spectral and attack features across 6 time bins by condition and cluster. (A) Spectral Centroid Mean, (B) Spectral Centroid Standard Deviation, (C) Attack Magnitude. Mean \pm SEM.

Additional frequency features relating to the magnitude of the fundamental frequency and its formants (F0 Magnitude Mean, F1 Magnitude Mean, F2 Magnitude Mean, F1/F0 Ratio, F2/F0 Ratio), with significant interactions but with smaller effect sizes, are presented in Supplementary material in section .1 (Supplementary Table .1 and Figures S9 and S10).

These features revealed distinctive patterns based on their acoustic properties. Magnitude features (F0 Magnitude Mean, F1 Magnitude Mean) demonstrated similar temporal inversion patterns. VPA exposure caused progressive declines specifically in cluster 1 calls across the recording session while control values increased, resulting in marked temporal inversions where VPA-treated chicks showed reduced magnitude in later time bins compared to controls (Figures S9 and S10). In contrast, ratio features (F1/F0 Ratio and F2/F0 Ratio) showed more stable temporal dynamics without dramatic inversions. VPA exposure

increased these ratios specifically in cluster 1 calls, with cluster 0 calls showing minimal condition-dependent changes. These patterns suggest that VPA exposure affects signal magnitude and spectral balance through distinct mechanisms, both selectively impacting cluster 1 calls (Figure S10).

4 Discussion

We introduced a computational framework that integrates call detection, multi-feature extraction, and unsupervised learning for the analysis of chicks' vocal repertoire. We first characterised the natural structure of chicks' early vocal repertoire by applying our approach to a dataset of newly-hatched untreated chicks. Clustering analyses revealed vocalisations distributed along a continuum between two main categories, rather than in discrete categories. Calls assigned to cluster 0 were shorter, lower in energy, and showed ascending frequency modulation, while calls assigned to cluster 1 were longer, louder, and displayed higher fundamental frequency values. Subcategories of calls are present within these two clusters, with more strongly supported subdivisions in cluster 0.

We then applied the framework to an independent dataset of chick calls [38], to understand whether prenatal VPA exposure affects early vocal production. Analyses confirmed the two-cluster continuum structure, with acoustic profiles resembling those in the development dataset. Calls in cluster 0 were shorter, with lower energy, whilst calls in cluster 1 were longer and louder, with higher frequency values. This consistency validated our approach's robustness whilst enabling assessment of systematic differences between control and VPA-exposed chicks.

Our approach overcomes historical constraints of manual annotation and predefined categories in chick vocalisation studies [15, 18], whilst ensuring reproducibility and scalability. By avoiding taxonomic priors, repertoire structure emerged directly from the data, thus avoiding classifier biases and unclassified calls that characterised supervised methods [17].

The framework leverages signal processing algorithms for accurate onset and offset call detection, rather than aggregating predictions over sliding windows that can capture incomplete calls and introduce temporal boundary errors [30], ensuring cleaner acoustic units. Finally, using a set of 20 mono-dimensional acoustic features across temporal, frequency, and energy domains captured variability beyond traditional prototypical call classifications (see Table S7, for a literature comparison), while ensuring interpretability, a critical balance often lost in black-box approaches. This broader acoustic space demonstrates the limitations of qualitative approaches and the value of data-driven methods for uncovering the full spectrum of natural vocal variation.

This study investigates prenatal VPA exposure effects on the early vocal repertoire of chicks, extending previous work on avian and mammalian models by revealing call-type specific feature differences [12, 62, 43, 14]. VPA-exposed chicks produced proportionally more cluster 0 calls and fewer cluster 1 calls, typically linked to contact calls for conspecifics. This parallels findings in marmosets [50], where VPA exposure altered call type distributions and disrupted parent-infant vocal interactions. This suggests that VPA affects specific call-types rather than uniformly disrupting vocal production across species [49, 43].

Feature analysis revealed systematic effects of VPA exposure with robust interactions between condition and call type across temporal, energy and frequency domains. In the temporal domain, VPA-exposed chicks showed reduced cluster 1 call duration. These findings align with rodent studies demonstrating that prenatal VPA exposure reduces call duration across developmental stages [52, 51].

In the energy domain, RMS Mean showed opposite trends across clusters: VPA-exposed chicks produced louder cluster 1 calls, but quieter cluster 0 calls. Similarly, in the frequency domain, cluster 1 calls in VPA-exposed chicks showed higher attack magnitudes, while cluster 0 calls had lower values. This bidirectional pattern suggests that VPA exposure disrupts normal energy regulation mechanisms,

leading to reduced intensity in softer calls whilst enhancing it in contact calls. These findings partially align with Nishigori et al. [44], where VPA-exposed chicks showed an overall call amplitude reduction compared to controls. However, methodological differences make direct comparisons difficult. Nishigori et al. [44] did not differentiate call types and analysed only call decibels. Further, they recorded chicks socially isolated after imprinting with conspecifics (post-hatching day P2-P4) [44], whereas we tested newly-hatched chicks (P0). Their overall intensity reduction [44] may therefore reflect specific call type changes, consistent with our cluster 0 energy reduction (Figure 7), which includes "soft calls" (see Table S7).

In the frequency domain, marked group differences in fundamental frequency variability emerged: in VPA-exposed chicks, cluster 1 calls showed consistently lower F0 standard deviation, slope, and 1st order difference, indicating reduced pitch variability and diminished dynamic modulation compared to controls. The F0 kurtosis was higher in VPA-exposed chicks for both clusters, reflecting less variable pitch distribution and flatter calls, with effects most pronounced in cluster 1. Finally, spectral centroid standard deviation was reduced in VPA-exposed chicks in both clusters, indicating decreased spectral variability. These alterations align with rodent models, where VPA exposure led to reduced call complexity and shifts toward simpler call types with altered peak frequency [52, 51, 43], but reveal call-type-specific vulnerability.

These findings show that the impact of prenatal VPA exposure is not uniform across the vocal repertoire and might indicate that VPA-exposed chicks show alterations in social communication that mirror those observed in social behaviour [45, 38, 47].

Since cluster 1 represents calls with greater acoustic variability and F0 modulation dynamics, further investigation must determine whether selective alterations originate from peripheral vocal production differences, motor impairments, or socio-cognitive and motivational deficits. Our experimental dataset was recorded during a social preference test with socially relevant stimuli, potentially eliciting specific vocalisation patterns. Interestingly, the average stimulus approach time (170-190 seconds) [38] coincides with increased call duration and intensity for cluster 1 calls (Figures 6 and 7), suggesting connections between social and motor responses and vocalisations requiring further investigations.

The computational framework addresses two major bottlenecks in bioacoustic research: the labour-intensive nature of manual annotation and the subjective biases in human-defined classification systems. Being inherently scalable and reproducible, our pipeline can process large datasets efficiently, making it suitable for longitudinal studies and high-throughput applications in neuroscientific research and precision livestock farming. Further, the framework's effectiveness with secondary data demonstrates transferability to existing datasets, facilitating the discovery of previously unexamined acoustic dimensions.

These findings position computational bioacoustics as an asset for neurodevelopmental research. Extended to other species and experimental contexts, this methodology can facilitate cross-species comparisons and advance understanding of conserved mechanisms underlying vocal communication disorders. As the field is moving toward more interdisciplinary approaches [21, 26], integrating acoustic analysis with neural substrate and behavioural tracking can comprehensively characterise developmental disorders.

Some limitations warrant consideration. Our six-minute recordings on the first day of hatching during a social preference test may have elicited specific vocalisation patterns, not reflecting the entire variety of vocal behaviour in these social animals. Future studies should investigate whether alterations persist

throughout development and in different contexts. Although our feature set covered temporal, frequency, and energy domains, higher-order features such as joint time-frequency scattering coefficients [37] could provide additional insight into potentially nonlinear acoustic interactions that could capture other vocal differences.

From a neuroscientific perspective, these results highlight how fine-grained vocal analysis can reveal subtle phenotypes in animal models of neurodevelopmental disorders and inform the investigation of neurobiological substrates underlying communication alterations. Avian models provide an ideal system for linking acoustic phenotypes to neural substrates and circuit-level mechanisms [14]. These results reinforce the value of domestic chicks as a model for studying innate vocal behaviour and demonstrate how computational bioacoustics can advance our understanding of neurodevelopmental conditions [12, 47, 46].

Data Availability

Dataset and code will be available upon acceptance via Zenodo (<https://doi.org/10.5281/zenodo.17880369>) and https://antorr91.github.io/Vpa_vocalisations_project/.

Author's Contributions

AMCT: Conceptualisation, Data curation, Formal analysis, Methodology, Software, Visualisation, Writing. IN: Software, Writing (review). PS: Conceptualisation, Data curation, Resources, Writing (review). EV: Conceptualisation, Methodology, Funding acquisition, Supervision, Writing (review). EB: Conceptualisation, Methodology, Funding acquisition, Project administration, Supervision, Software, Writing (review).

Funding

IN has been supported by a BBSRC grant (BB/S003223/1); PS has been supported by the Italian Ministry of University of Research (PS, Grant number 2022LJZRBY; EV has been supported by a Royal Society Leverhulme Trust Senior Research Fellowship (SRF\R1\210001155), a Leverhulme Trust grant (RPG-2020-287) and a BBSRC grant (BB/S003223/1); EB has been supported by a RAEEng/Leverhulme Trust Research Fellowship (LTRF2223-19-106).

Ethics Statement

Experimental procedures adhered to national regulations on animal research. For the experimental dataset, procedures were approved by the University of Trento ethical committee and authorised by the Italian Ministry of Health (permit no. 1060/2015-PR), in accordance with EU Directive 2010/63/EU. For the Development dataset, procedures were approved by the Queen Mary University of London ethics committee (AWERB) and Home Office (PP5180959).

Acknowledgements

We thank Michael Emmerson, Laura Freeland, and Shuge Wang for their assistance with the annotation of the Development dataset.

References

- [1] Edgar J, Held S, Jones C, Troisi C 2016 Influences of maternal care on chicken welfare. *Animals* **6**, 2 doi:10.3390/ani6010002.
- [2] Andrew R 1969 Intracranial self-stimulation in the chick and the causation of emotional behavior. *Annals of the New York Academy of Sciences* **159**, 625–639 doi:10.1111/j.1749-6632.1969.tb12967.x.
- [3] Briefer EF 2020 Coding for ‘dynamic’ information: vocal expression of emotional arousal and valence in non-human animals. *Coding strategies in vertebrate acoustic communication* pp. 137–162 doi:10.1007/978-3-030-39200-0_6.
- [4] Manteuffel G, Puppe B, Schön PC 2004 Vocalization of farm animals as a measure of welfare. *Applied Animal Behaviour Science* **88**, 163–182 doi:10.1016/j.applanim.2004.02.012.
- [5] Herborn KA, McElligott AG, Mitchell MA, Sandilands V, Bradshaw B, Asher L 2020 Spectral entropy of early-life distress calls as an iceberg indicator of chicken welfare. *Journal of the Royal Society Interface* **17**, 20200086 doi:10.1098/rsif.2020.0086.
- [6] Laurijs KA, Briefer EF, Reimert I, Webb LE 2021 Vocalisations in farm animals: A step towards positive welfare assessment. *Applied Animal Behaviour Science* **236**, 105264 doi:10.1016/j.applanim.2021.105264.
- [7] Bist RB, Bist K, Poudel S, Subedi D, Yang X, Paneru B, Mani S, Wang D, Chai L 2024 Sustainable poultry farming practices: A critical review of current strategies and future prospects. *Poultry Science* p. 104295 doi:10.1016/j.psj.2024.104295.
- [8] Özentürk U, Chen Z, Jamone L, Versace E 2024 Robotics for poultry farming: Challenges and opportunities. *Computers and Electronics in Agriculture* **226**, 109411 doi:10.1016/j.compag.2024.109411.
- [9] Di Giorgio E, Loveland JL, Mayer U, Rosa-Salva O, Versace E, Vallortigara G 2017 Filial responses as predisposed and learned preferences: Early attachment in chicks and babies. *Behavioural brain research* **325**, 90–104 doi:10.1016/j.bbr.2016.09.018.
- [10] McCabe BJ 2019 Visual imprinting in birds: behavior, models, and neural mechanisms. *Frontiers in Physiology* **10**, 658 doi:10.3389/fphys.2019.00658.
- [11] Nicol CJ 2015 *The behavioural biology of chickens*. Cabi doi:10.1016/j.anbehav.2016.04.018.
- [12] Matsushima T, Izumi T, Vallortigara G 2024 The domestic chick as an animal model of autism spectrum disorder: building adaptive social perceptions through prenatally formed predispositions. *Frontiers in Neuroscience* **18**, 1279947 doi:10.3389/fnins.2024.1279947.

- [13] Versace E, Ragusa M, Vallortigara G 2019 A transient time window for early predispositions in newborn chicks. *Scientific Reports* **9**, 18767 doi:10.1101/623439.
- [14] Csillag A, Ádám Á, Zachar G 2022 Avian models for brain mechanisms underlying altered social behavior in autism. *Frontiers in physiology* **13**, 1032046 doi:10.3389/fphys.2022.1032046.
- [15] Collias N, Joos M 1953 The spectrographic analysis of sound signals of the domestic fowl. *Behaviour* pp. 175–188 doi:10.1163/156853953x00104.
- [16] Fontana I, Tullo E, Butterworth A, Guarino M 2015 An innovative approach to predict the growth in intensive poultry farming. *Computers and electronics in agriculture* **119**, 178–183 doi:10.1016/j.compag.2015.10.001.
- [17] Thomas P, Grzywalski T, Hou Y, de Carvalho PS, De Gussem M, Antonissen G, Tuyttens F, De Poorter E, Devos P, Botteldooren D 2023 Using a Neural Network based Vocalization Detector for Broiler Welfare Monitoring. In *10th Convention of the European Acoustics Association* doi:10.61782/fa.2023.0474.
- [18] Marx G, Leppelt J, Ellendorff F 2001 Vocalisation in chicks (*Gallus gallus dom.*) during stepwise social isolation. *Applied Animal Behaviour Science* **75**, 61–74 doi:10.1016/s0168-1591(01)00180-0.
- [19] Collins SA, Herborn K, Sufka KJ, Asher L, Brilot B 2024 Do I sound anxious? Emotional arousal is linked to changes in vocalisations in domestic chicks (*Gallus gallus dom.*). *Applied Animal Behaviour Science* **277**, 106359 doi:10.1016/j.applanim.2024.106359.
- [20] de Carvalho Soster P, Grzywalski T, Hou Y, Thomas P, Dedeurwaerder A, De Gussem M, Tuyttens F, Devos P, Botteldooren D, Antonissen G 2025 Automated detection of broiler vocalizations a machine learning approach for broiler chicken vocalization monitoring. *Poultry Science* **104**, 104962 doi:10.1016/j.psj.2025.104962.
- [21] Sainburg T, Gentner TQ 2021 Toward a computational neuroethology of vocal communication: from bioacoustics to neurophysiology, emerging tools and future directions. *Frontiers in Behavioral Neuroscience* **15**, 811737 doi:10.3389/fnbeh.2021.811737.
- [22] Stowell D, Wood M, Stylianou Y, Glotin H 2016 Bird detection in audio: a survey and a challenge. In *2016 IEEE 26th International Workshop on Machine Learning for Signal Processing (MLSP)* pp. 1–6. IEEE doi:10.1109/mlsp.2016.7738875.
- [23] Stowell D 2022 Computational bioacoustics with deep learning: a review and roadmap. *PeerJ* **10**, e13152 doi:10.7717/peerj.13152.
- [24] Xie J, Zhong Y, Zhang J, Liu S, Ding C, Triantafyllopoulos A 2023 A review of automatic recognition technology for bird vocalizations in the deep learning era. *Ecological Informatics* **73**, 101927 doi:10.1016/j.ecoinf.2022.101927.
- [25] Noumida A, Rajan R 2022 Multi-label bird species classification from audio recordings using attention framework. *Applied Acoustics* **197**, 108901 doi:10.1016/j.apacoust.2022.108901.

[26] Robinson D, Miron M, Hagiwara M, Pietquin O 2024 NatureLM-audio: an Audio-Language Foundation Model for Bioacoustics. *arXiv preprint arXiv:2411.07186* doi:10.1109/icassp49660.2025.10888629.

[27] Stowell D, Plumbley MD 2014 Automatic large-scale classification of bird sounds is strongly improved by unsupervised feature learning. *PeerJ* **2** doi:10.7717/peerj.488.

[28] Van Engelen JE, Hoos HH 2020 A survey on semi-supervised learning. *Machine learning* **109**, 373–440 doi:10.1007/s10994-019-05855-6.

[29] Nolasco I, Singh S, Morfi V, Lostanlen V, Strandburg-Peshkin A, Vidaña-Vila E, Gill L, Pamuła H, Whitehead H, Kiskin I et al. 2023 Learning to detect an animal sound from five examples. *Ecological informatics* **77**, 102258 doi:10.1016/j.ecoinf.2023.102258.

[30] Grzywalski T, de Carvalho PS, Hou Y, Thomas P, Tuyttens FA, Dedeurwaerder A, De Gussem M, Devos P, Antonissen G, Botteldooren D 2025 Identification and Characterization of Clusters of Potentially New Vocalizations in Broiler Chickens Using Advanced Acoustic Analysis. *Poultry Science* p. 105769 doi:10.1016/j.psj.2025.105769.

[31] Moummad I, Farrugia N, Serizel R 2024 Self-supervised learning for few-shot bird sound classification. In *2024 IEEE International Conference on Acoustics, Speech, and Signal Processing Workshops (ICASSPW)* pp. 600–604. IEEE doi:10.1109/icasspw62465.2024.10627576.

[32] Goffinet J, Brudner S, Mooney R, Pearson J 2021 Low-dimensional learned feature spaces quantify individual and group differences in vocal repertoires. *Elife* **10**, e67855 doi:10.7554/elife.67855.

[33] Sainburg T, Thielk M, Gentner TQ 2020 Finding, visualizing, and quantifying latent structure across diverse animal vocal repertoires. *PLoS computational biology* **16**, e1008228 doi:10.1371/journal.pcbi.1008228.

[34] Rokach L, Maimon O, Shmueli E 2023 *Machine Learning for Data Science Handbook*. Springer doi:10.1007/978-3-031-24628-9.

[35] Elie JE, Theunissen FE 2016 The vocal repertoire of the domesticated zebra finch: a data-driven approach to decipher the information-bearing acoustic features of communication signals. *Animal cognition* **19**, 285–315 doi:10.1007/s10071-015-0933-6.

[36] Fischer J, Wadewitz P, Hammerschmidt K 2017 Structural variability and communicative complexity in acoustic communication. *Animal Behaviour* **134**, 229–237 doi:10.1016/j.anbehav.2016.06.012.

[37] Wang C, Benetos E, Wang S, Versace E 2022 Joint scattering for automatic chick call recognition. In *2022 30th European Signal Processing Conference (EUSIPCO)* pp. 195–199. IEEE doi:10.23919/eusipco55093.2022.9909738.

[38] Lorenzi E, Pross A, Rosa-Salva O, Versace E, Sgadò P, Vallortigara G 2019 Embryonic exposure to valproic acid affects social predispositions for dynamic cues of animate motion in newly-hatched chicks. *Frontiers in Physiology* **10**, 501 doi:10.3389/fphys.2019.00501.

[39] Johannessen CU, Johannessen SI 2003 Valproate: past, present, and future. *CNS drug reviews* **9**, 199–216 doi:10.1111/j.1527-3458.2003.tb00249.x.

[40] Christensen J, Grønborg TK, Sørensen MJ, Schendel D, Parner ET, Pedersen LH, Vestergaard M 2013 Prenatal valproate exposure and risk of autism spectrum disorders and childhood autism. *Jama* **309**, 1696–1703.

[41] Kataoka S, Takuma K, Hara Y, Maeda Y, Ago Y, Matsuda T 2013 Autism-like behaviours with transient histone hyperacetylation in mice treated prenatally with valproic acid. *International journal of Neuropsychopharmacology* **16**, 91–103 doi:10.1017/s1461145711001714.

[42] Roullet FI, Lai JK, Foster JA 2013 In utero exposure to valproic acid and autism—a current review of clinical and animal studies. *Neurotoxicology and teratology* **36**, 47–56 doi:10.1016/j.ntt.2013.01.004.

[43] Nicolini C, Fahnestock M 2018 The valproic acid-induced rodent model of autism. *Experimental neurology* **299**, 217–227 doi:10.1016/j.expneurol.2017.04.017.

[44] Nishigori H, Kagami K, Takahashi A, Tezuka Y, Sanbe A, Nishigori H 2013 Impaired social behavior in chicks exposed to sodium valproate during the last week of embryogenesis. *Psychopharmacology* **227**, 393–402 doi:10.1007/s00213-013-2979-y.

[45] Sgadò P, Rosa-Salva O, Versace E, Vallortigara G 2018 Embryonic exposure to valproic acid impairs social predispositions of newly-hatched chicks. *Scientific reports* **8**, 5919 doi:10.1038/s41598-018-24202-8.

[46] Zachar G, Tóth AS, Gerecsei LI, Zsebők S, Ádám Á, Csillag A 2019 Valproate exposure in ovo attenuates the acquisition of social preferences of young post-hatch domestic chicks. *Frontiers in physiology* **10**, 881 doi:10.3389/fphys.2019.00881.

[47] Adiletta A, Pedrana S, Rosa-Salva O, Sgadò P 2021 Spontaneous visual preference for face-like stimuli is impaired in newly-hatched domestic chicks exposed to valproic acid during embryogenesis. *Frontiers in Behavioral Neuroscience* **15**, 733140 doi:10.3389/fnbeh.2021.733140.

[48] Adiletta A, Pross A, Taricco N, Sgadò P 2022 Embryonic valproate exposure alters mesencephalic dopaminergic neurons distribution and septal dopaminergic gene expression in domestic chicks. *Frontiers in Integrative Neuroscience* **16**, 804881 doi:10.3389/fnint.2022.804881.

[49] Uesaka M, Kawauchi H, Yamaoka K, Wakabayashi Y, Kinoshita Y, Ono N, Noguchi J, Watanabe S, Ichinohe N, Benner S et al. 2023 Automatic Call Classification of Autism Model Marmosets by Deep Learning and Analysis of Their Vocal Development. In *2023 Asia Pacific Signal and Information Processing Association Annual Summit and Conference (APSIPA ASC)* pp. 2233–2237. IEEE doi:10.1109/apsipaasc58517.2023.10317121.

[50] Mimura K, Nakagaki K, Morishita H, Ichinohe N 2025 Altered kinship vocal dynamics in marmosets with valproic acid-induced model of autism. *bioRxiv* pp. 2025–01 doi:10.1101/2025.01.30.635822.

[51] Moldrich RX, Leanage G, She D, Dolan-Evans E, Nelson M, Reza N, Reutens DC 2013 Inhibition of histone deacetylase in utero causes sociability deficits in postnatal mice. *Behavioural brain research* **257**, 253–264 doi:10.1016/j.bbr.2013.09.049.

[52] Gzielo K, Potasiewicz A, Hołuj M, Litwa E, Popik P, Nikiforuk A 2020 Valproic acid exposure impairs ultrasonic communication in infant, adolescent and adult rats. *European neuropsychopharmacology* **41**, 52–62 doi:10.1016/j.euroneuro.2020.09.006.

[53] Cannam C, Landone C, Sandler MB, Bello JP 2006 The Sonic Visualiser: A Visualisation Platform for Semantic Descriptors from Musical Signals.. In *ISMIR* pp. 324–327.

[54] Audacity T 2017 Audacity. *The name audacity (R) is a registered trademark of dominic mazzoni* retrieved from <http://audacity.sourceforge.net>.

[55] Torrisi A, De Almeida Nolasco IS, Versace E, Benetos E 2024 Exploratory analysis of early-life chick calls. In *Proceedings of the 4th International Workshop on Vocal Interactivity in-and-between Humans, Animals and Robots (VIHAR 2024)*.

[56] Müller M 2015 *Fundamentals of Music Processing: Audio, Analysis, Algorithms, Applications*. Cham: Springer doi:10.1007/978-3-319-21945-5.

[57] Mauch M, Dixon S 2014 pYIN: A fundamental frequency estimator using probabilistic threshold distributions. In *2014 IEEE International Conference on Acoustics, Speech and Signal Processing (ICASSP)* pp. 659–663. IEEE doi:10.1109/icassp.2014.6853678.

[58] Panagiotakis C, Tzirtiras G 2005 A speech/music discriminator based on RMS and zero-crossings. *IEEE Transactions on Multimedia* **7**, 155–166 doi:10.1109/TMM.2004.840604.

[59] Virtanen T, Plumley MD, Ellis D 2018 *Computational analysis of sound scenes and events*. Springer.

[60] Zadeh LA 2008 Is there a need for fuzzy logic?. *Information sciences* **178**, 2751–2779 doi:10.1016/s0020-7373(79)80036-x.

[61] Harrison XA, Donaldson L, Correa-Cano ME, Evans J, Fisher DN, Goodwin CE, Robinson BS, Hodgson DJ, Inger R 2018 A brief introduction to mixed effects modelling and multi-model inference in ecology. *PeerJ* **6**, e4794 doi:10.7717/peerj.4794.

[62] Tewelde EG, Morvai B, Zachar G, Pogány Á 2025 Prenatal Valproic Acid Exposure Affects Song Learning in Zebra Finches: A Potential Model for Vocal Development in Autism. *Life* **15**, 1058 doi:10.3390/life15071058.

[63] Böck S, Widmer G 2013 Maximum filter vibrato suppression for onset detection. In *Proc. of the 16th Int. Conf. on Digital Audio Effects (DAFx). Maynooth, Ireland (Sept 2013)* vol. 7 p. 4 doi:10.1121/1.4894272.

[64] Mesaros A, Heittola T, Virtanen T 2016 Metrics for polyphonic sound event detection. *Applied Sciences* **6**, 162 doi:10.3390/app6060162.

[65] Raffel C, McFee B, Humphrey EJ, Salamon J, Nieto O, Liang D, Ellis DP, Raffel CC 2014
MIR_EVAL: A Transparent Implementation of Common MIR Metrics.. In *ISMIR* vol. 10 p. 2014.

Supplementary material

S1. Extended Methods

This section provides detailed methodological procedures that complement the main Methods section.

S1.1 Onset and Offset Detection

We used the best onset and offset detection algorithms identified in a previous study conducted on the development dataset [55].

For onset detection, the High Frequency Content (HFC) algorithm [56] was selected based on its superior performance compared to other algorithms tested, including phase and amplitude-based methods (Thresholded Phase Deviation, Normalised Weighted Phase Deviation, and Rectified Complex Domain [56]) and energy-based methods like Superflux [63]. The HFC algorithm detects frequency changes within the signal, making it particularly suited for identifying the sharp spectral transitions characteristic of chick vocalisation onsets.

For offset detection, we implemented three methods operating within a predefined time window based on the maximum expected duration of chick calls: (i) local minimum detection of the energy signal, (ii) first-order differencing of the energy signal followed by local minimum detection, and (iii) second-order differencing combined with local minimum detection. The first-order differencing method was selected based on its superior performance compared to the other approaches tested. Performance evaluation on the development dataset and benchmarking results on the experimental dataset are presented in Section 4.

S1.2 Onset and Offset Detection Performance

S1.2.1 Evaluation Metrics

To evaluate onset and offset detection performance, predicted events were compared to manually annotated ground-truth labels using event-based metrics [64]. A prediction was considered a True Positive (TP) if it fell within a defined tolerance window relative to the ground-truth. For the onset detection task, a fixed tolerance window of 100 ms (± 50 ms) was used, based on preliminary qualitative analysis that confirmed this threshold as optimal for chick calls. For the offset detection task, an adaptive tolerance window was used. While a fixed 100 ms window was applied by default, for longer events the tolerance was set to half the total event duration (e.g., 150 ms for a 300 ms call), to account for the greater temporal variability typically associated with offset annotations in vocalisations of variable length. Predicted offsets were estimated using the corresponding predicted onset as an anchor and evaluated call-wise against the corresponding ground truth offsets. Undetected vocalisations were counted as False Negatives (FN), while extra or duplicated detections were considered False Positives (FP). Evaluation metrics were computed using the `onset.evaluate` function from the `mir_eval` Python library [65]:

1. **Precision:** Represents the ratio of True Positives against all instances estimated as positive, including False Positives

$$\text{Precision} = \frac{\text{True Positives}}{\text{True Positives} + \text{False Positives}}$$

2. **Recall (Sensitivity):** Ratio of True Positives to all actual positives (True Positives + False Negatives).

$$\text{Recall} = \frac{\text{True Positives}}{\text{True Positives} + \text{False Negatives}}$$

3. **F1-measure:** Combines Precision and Recall, producing a unified measure (the harmonic mean). The F1-measure provides insight into both the model's capacity to make accurate positive predictions and its

capacity to capture all real positive instances.

$$F1 = \frac{2 \cdot \text{Precision} \cdot \text{Recall}}{\text{Precision} + \text{Recall}}$$

These metrics were computed individually for each audio file and aggregated using weighted averages to handle the imbalanced distribution of calls within each audio file:

$$\text{Metric}_{\text{weighted}} = \sum_{i=1}^N w_i \cdot \text{Metric}_i$$

S1.2.2 Results Detection Performance Across Datasets

To ensure the robustness and generalisability of the automatic detection system, onset and offset detection were evaluated on both the development dataset and on the experimental dataset for benchmarking. In Table S1, detection performances are presented across both datasets.

Dataset	Detection Type	Weighted F1-measure	Weighted Precision	Weighted Recall
Development Dataset (31 naïve chicks)	Onset (HFC)	0.853	0.908	0.841
Development Dataset (31 naïve chicks)	Offset (1st-order difference)	0.724	0.724	0.724
Experimental Dataset (46 chicks: 27 VPA / 19 control)	Onset (HFC)	0.933	0.910	0.961
Experimental Dataset (46 chicks: 27 VPA / 19 control)	Offset (1st-order difference)	0.885	0.885	0.885

Table S1: Performance metrics for automatic onset and offset detection across datasets. HFC = High Frequency Content algorithm; 1st-order difference = First order difference of energy + local minimum detection.

The results confirmed the effectiveness of the automatic detection methods on the complete experimental dataset. Onset detection performed consistently well across datasets, with improved performance in the experimental Dataset ($F1 = 0.933$) compared to the development Dataset ($F1 = 0.853$). Similarly, offset detection showed substantial improvement in the experimental Dataset ($F1 = 0.885$) compared to the development Dataset ($F1 = 0.724$), likely reflecting better signal quality for the audio recorded for the experimental dataset.

These results validated the use of automated detection in this study. The high precision and recall values demonstrate the reliability of our method for large-scale signal analysis.

S2. Features extracted for the chicks' calls analysis

Before feature extraction, a bandpass filter (BPF) was applied to each recording to reduce background noise and focus on the frequency bands relevant to chick vocalisations, specifically the fundamental frequency along with its first and second harmonics. The frequency range of the filter was set to 2000-12,600 Hz for the development dataset and to 2000-15,000 Hz for the experimental dataset, to account for range differences.

For each segmented call, we extracted different components of the signal. The Fundamental Frequency (F0), indicating the average number of oscillations per second (in Hz), was estimated using the PYIN algorithm [57]. From this estimate, frequency bins corresponding to the first and second harmonics (F1 and F2) were derived [56], and their magnitudes computed via the Fast Fourier Transform (FFT), with normalisation relative to the sampling frequency. We then computed the Root Mean Square (RMS) [58], which measures the signal energy and provides an estimate of its overall intensity, and the Spectral Centroid, which represents the weighted average of frequencies in the signal spectrum. For the Spectral Centroid [56], we focused on the typical frequency band of chick vocalisations, between 2000 Hz and 12,600 Hz. The signal envelope [59] was derived by segmenting the waveform of each call and applying the Hilbert transform to compute the analytic signal, from which the absolute amplitude was extracted.

From these signal-level features, we characterised each call by calculating 20 one-dimensional statistical descriptors. These are grouped into: temporal domain features (Call Duration, Attack Time, Envelope Slope), frequency domain features (F0 Mean, F0 Standard Deviation, F0 Kurtosis, F0 Skewness, F0 Bandwidth, F0 Slope, F0 1st Order Difference Mean, F0 Mag Mean, F1 Mag Mean, F2 Mag Mean, F0-F1 Mean Ratio, F0-F2 Mean Ratio, Spectral Centroid Mean and Spectral Centroid Standard Deviation, Attack Magnitude), and energy domain features (RMS Mean, RMS Standard Deviation). Detailed feature descriptions and equations to derive them are provided in Table S2. The implementation code used to derive these features is publicly accessible at the following link¹, supporting transparency and reproducibility of the signal processing pipeline. All extracted features were z-score normalised prior to clustering, ensuring they were on a comparable scale for these analyses.

¹https://github.com/antorr91/Chicks_exploratory_study/blob/main/feature_extraction_functions.py

Feature	Definition	Equation
Call Duration (T)	Time difference between the offset and onset of a call.	$T_{\text{end}} - T_{\text{start}}$
F0 Mean (F)	Average fundamental frequency within the call.	$\frac{1}{N} \sum_{i=1}^N F0_i$
F0 Std Dev (F)	Variability of fundamental frequency values within the call.	$\sqrt{\frac{1}{N-1} \sum_{i=1}^N (F0_i - \bar{F0})^2}$
F0 Skewness (F)	Symmetry of the F0 distribution (positive = right-skewed).	$\frac{\frac{1}{N} \sum_{i=1}^N (F0_i - \bar{F0})^3}{\left(\sqrt{\frac{1}{N} \sum_{i=1}^N (F0_i - \bar{F0})^2}\right)^3}$
F0 Kurtosis (F)	Peakedness or flatness of the F0 distribution (positive value = heavier tails, irregular modulation; negative value = lighter tails, smoother modulation).	$\frac{\frac{1}{N} \sum_{i=1}^N (F0_i - \bar{F0})^4}{\left(\sqrt{\frac{1}{N} \sum_{i=1}^N (F0_i - \bar{F0})^2}\right)^4} - 3$
F0 Bandwidth (F)	Range or span of F0 values within a call.	$\max(F0) - \min(F0)$
Mean of F0's First-Order Difference (F)	Average of differences between consecutive F0 values.	$\frac{1}{N-1} \sum_{i=2}^N (F0_i - F0_{i-1})$
F0 Slope (F)	Rate of frequency change from onset to peak.	$\frac{F0_{\text{peak}} - F0_{\text{onset}}}{T_{\text{attack}}}$
F0 Magnitude Mean (F)	Average intensity of the fundamental frequency.	$\frac{1}{N} \sum_{i=1}^N X(F0_i) $
F1 Magnitude Mean (F)	Average intensity of the first harmonic.	$\frac{1}{N} \sum_{i=1}^N X(F1_i) $
F2 Magnitude Mean (F)	Average intensity of the second harmonic.	$\frac{1}{N} \sum_{i=1}^N X(F2_i) $
Ratio F0/F1 Magnitude Mean (F)	Ratio of the intensity of F0 to F1.	$\frac{ X(F0) }{ X(F1) }$
Ratio F0/F2 Magnitude Mean (F)	Ratio of the intensity of F0 to F2.	$\frac{ X(F0) }{ X(F2) }$
Spectral Centroid Mean (F)	Average spectral centroid.	$\frac{1}{N} \sum_{t=1}^N \frac{\sum_{k=1}^K f_k \cdot X(f_k, t) }{\sum_{k=1}^K X(f_k, t) }$
Spectral Centroid Std Dev (F)	Variability of spectral centroid values.	$\sqrt{\frac{1}{N-1} \sum_{t=1}^N (SC_t - \bar{SC})^2}$
RMS Mean (E)	Average RMS value indicating overall energy.	$\frac{1}{N} \sum_{i=1}^N RMS_i$
RMS Std Dev (E)	Variability of RMS values.	$\sqrt{\frac{1}{N-1} \sum_{i=1}^N (RMS_i - \bar{RMS})^2}$
Attack Magnitude of the Envelope (F)	Intensity of the attack of the call.	$ x(t_{\text{peak}}) - x(t_{\text{onset}}) $
Attack Time of the Envelope (T)	Duration from onset to peak amplitude.	$t_{\text{peak}} - t_{\text{onset}}$
Slope of the Envelope (T)	Rate of change of amplitude during attack.	$\frac{ x(t_{\text{peak}}) - x(t_{\text{onset}}) }{t_{\text{peak}} - t_{\text{onset}}}$

Table S2: Extracted features for the exploratory study. (T)= Time-domain, (E)= Energy domain, (F)= Frequency-domain

S3. Clustering analysis

For the analysis of chicks' vocal repertoire, we evaluated hard and soft clustering methods to capture potentially different underlying structures. Hard clustering techniques, where each instance belongs to only one cluster, are well-suited for identifying discrete categories [36]. We tested three hard clustering techniques: K-means [34], Hierarchical Agglomerative Clustering (HAC)[34], and Density-Based Spatial Clustering of Applications with Noise (DBSCAN) [34]. In contrast, soft clustering techniques allow each instance to belong to multiple clusters, making them more appropriate when the data exhibit a continuous distribution[60]. We tested two soft clustering techniques: Fuzzy C-Means [34] and Gaussian Mixture Models (GMMs) [34].

To identify the optimal clustering structure for the development dataset, we performed a grid search, testing solutions with 1 to 10 clusters for each algorithm. Three metrics guided optimisation: (i) Silhouette Score [34]: quantifies how similar each point is to its own cluster compared to others; (ii) Within Cluster Sum of Squares (WCSS) [34] used with the Elbow method to identify the point beyond which adding more clusters does not significantly improve compactness; (iii) Calinski-Harabasz Index (CHI, or Variance Ratio Criterion, VRC) [34]: evaluates the ratio of dispersion between and within clusters. For soft clustering, we used additional metrics: Fuzzy Partition Coefficient (FPC)[34], which evaluates the quality of fuzzy separation (for Fuzzy C-Means); Akaike Information Criterion (AIC) [34] and Bayesian Information Criterion (BIC) [34] that balance model fit and complexity (for GMM). For finding the optimal clustering division, the same grid search optimisation approach and evaluation metrics were used for the experimental dataset.

Following the quantitative analysis, we validated the clustering results through qualitative analysis by examining calls at different distances from the cluster centroid, assessing internal consistency and identifying potential outliers. We assessed internal consistency using a percentile-based sampling method. Calls within each cluster were ranked based on their Euclidean distance from the cluster centroids, which represent the mean acoustic profile of the cluster distribution. Given the higher performance of HAC in terms of internal consistency, fewer outliers and interpretability, we report the results of this clustering method.

For HAC, we employed Ward linkage, which minimises the increase in within-cluster variance when merging clusters and is suited for a multi-dimensional acoustic feature space. To visualise this hierarchical clustering structure for both datasets, we generated dendograms, where branch height represents the Ward distance at which clusters are merged

S3.1 Clustering analysis results on the Development Dataset

This section summarises the comparative evaluation of clustering methods applied to the vocalisations of naïve chicks, recorded 12 hours after hatching. Although grid search optimisation was performed for cluster numbers ranging from $K = 2$ to $K = 10$, only the most informative solutions ($K \leq 5$) are reported here, as higher values consistently yielded diminishing returns across all metrics.

Clustering performance was assessed using the internal validity metrics described in the Methods section. The results for each algorithm and cluster number are summarised in Table S3.

The clustering results indicate that the optimal number of clusters depends on the method and evaluation metrics.

For $K = 2$, K-means, Fuzzy C-means, and HAC show strong internal consistency (Silhouette: 0.2621–0.2935, CHI: 1820.717–2075.166), but the structure is simplistic. GMM performs poorly (Silhouette: 0.1635, CHI: 665.4113), while DBSCAN has the highest Silhouette (0.6126) but a low CHI (32.8501), suggesting it captures local density rather than a global structure.

For $K = 3$, GMM improves (Silhouette: 0.1895, CHI: 897.0853), balancing cluster quality and model complexity. AIC/BIC values (AIC: 40338.0000, BIC: 82395.33) further support this choice. Fuzzy C-means and K-means remain stable (Silhouette: 0.2053–0.2056, CHI: 1431.661–1444.536), with FCM achieving the lowest

Cluster	Method	Silhouette Score	CHI	WCSS	Soft clustering metrics
2	K-means	0.293544	2075.165721	87736.037814	-
2	Fuzzy C-means	0.292199	2064.470661	57202.438842	FPC: 0.618044
2	HAC	0.262055	1820.717257	90619.163365	-
2	GMM	0.163535	665.411260	106512.447792	BIC: 85477.93, AIC: 82395.33
2	DBSCAN	0.612587	32.850100	99294.292399	-
3	K-means	0.205640	1444.535753	79627.221719	-
3	Fuzzy C-means	0.205255	1431.660788	37624.026316	FPC: 0.423804
3	HAC	0.173450	1214.278693	84018.834471	-
3	GMM	0.189538	897.085339	90928.248410	BIC: 82395.33, AIC: 40338.25
3	DBSCAN	0.541936	36.791861	102265.344510	-
4	K-means	0.218570	1242.981469	72692.093594	-
4	Fuzzy C-means	0.179696	931.787190	28213.933835	FPC: 0.318023
4	HAC	0.175407	989.556403	78909.630165	-
4	GMM	0.175460	948.214865	80026.578493	BIC: 18210.01, AIC: 12038.12
4	DBSCAN	0.480605	16.904633	101784.735236	-
5	K-means	0.185797	1087.206512	68299.126302	-
5	Fuzzy C-means	-0.030367	646.790263	22638.646939	FPC: 0.253115
5	HAC	0.132163	893.086602	73886.579398	-
5	GMM	0.087556	740.931014	78949.551308	BIC: 4527.62, AIC: -3188.90
5	DBSCAN	0.366437	12.984974	97517.557780	-

Table S3: Clustering performance metrics for $K = 2$ to $K = 5$. FPC = Fuzzy Partition Coefficient; AIC = Akaike Information Criterion; BIC = Bayesian Information Criterion; CHI = Calinski-Harabasz Index; WCSS = Within-Cluster Sum of Squares. Bold values indicate optimal scores per metric. The best clusters for WCSS were determined using the Elbow method.

WCSS (37624.0263), indicating well-defined clusters.

For $K = 4$, WCSS further decreases (28213.9338 in FCM), but FPC drops (0.318), suggesting more cluster overlap. GMM continues to reduce AIC/BIC (AIC: 12038.0000, BIC: 18210.0000), yet Silhouette scores remain stagnant (0.1755), indicating that increasing K does not improve separation.

Overall, these findings support that the selection of a two-cluster solution provides the best balance between separation and complexity.

S3.2 Clustering analysis results on the Experimental Groups

We applied Hierarchical Agglomerative Clustering (HAC) independently to the VPA and control groups in the experimental dataset. For the VPA-treated group, the Silhouette Score peaked at $K = 2$ (0.425), indicating that vocalisations were best distinguished at a broader categorical level. The CHI peaked at $K = 2$ (1724.68) and declined thereafter, further supporting the presence of two primary vocalisation categories. However, the bending method applied to WCSS identified $K = 5$ (WCSS = 206842.54) as the optimal number of clusters, suggesting a possible substructure in the data. Despite this, the relatively low Silhouette Score at $K = 5$ (0.126) suggested poor

cluster separation. This is consistent with a more continuous organisation of vocal features rather than sharply defined categories.

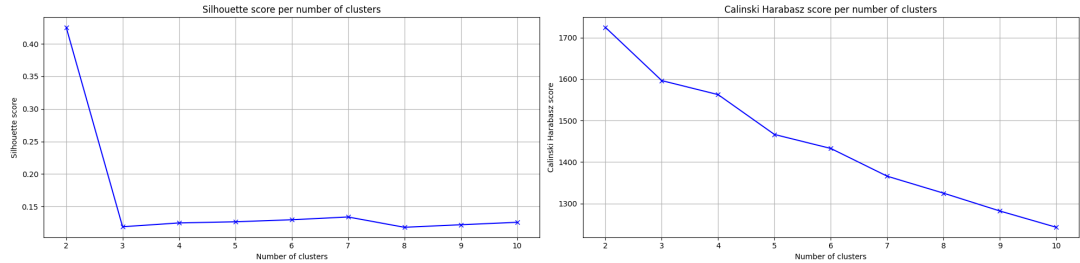


Figure S1: Clustering performance metrics for the VPA group across cluster solutions ($K = 2$ to $K = 10$). Silhouette Score and CHI peak at $K = 2$.

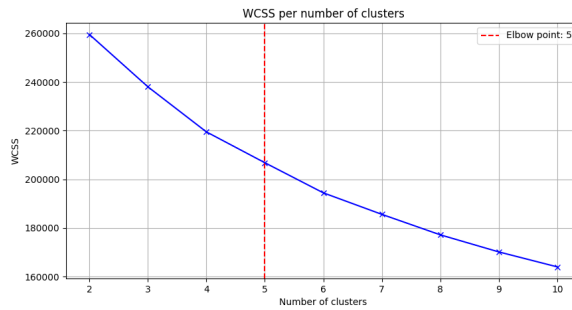


Figure S2: Within-Cluster Sum of Squares (WCSS) for the VPA group. The Elbow method suggests an inflection at $K = 5$.

Similarly, for control chicks, the highest Silhouette Score was observed at $K = 2$ (0.393), while $K = 3$ (0.347) also provided a reasonable balance between separation and model complexity. The CHI index was highest at $K = 2$ (1820.28), indicating strong structural differentiation at this level. Although the Elbow method indicated that $K = 5$ (WCSS = 120806.51) was optimal based on WCSS trends, as seen in the VPA group, the low Silhouette Score at $K = 5$ (0.120) suggested significant cluster overlap and an implausible cluster structure for this partitioning.

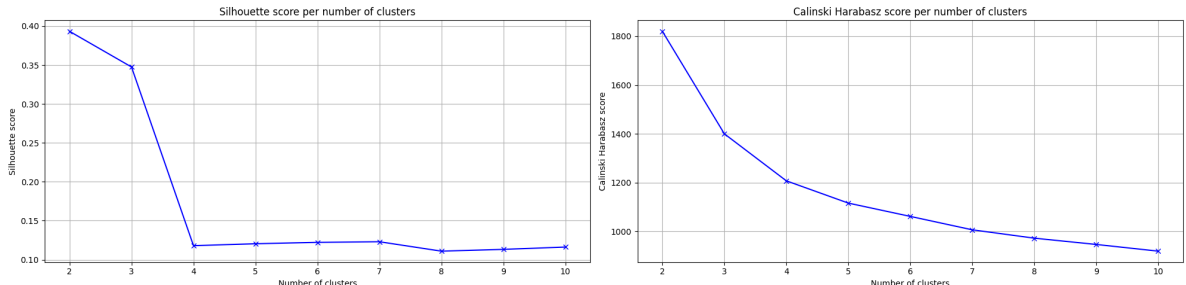


Figure S3: Clustering performance metrics for the control group. Both Silhouette Score and CHI are highest at $K = 2$.

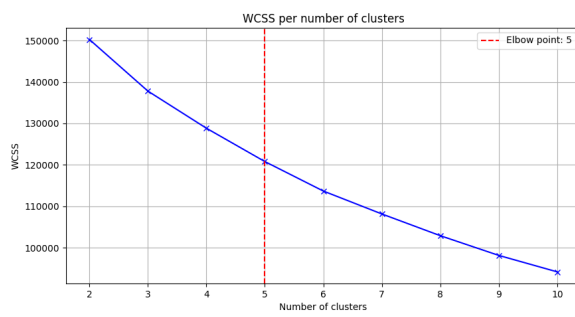


Figure S4: Within-Cluster Sum of Squares (WCSS) for the control group. The elbow is observed at $K = 5$.

S4. Non-linear 2D UMAP of Experimental Groups' calls

To visualise group structure without imposing linear assumptions, we embedded the 20 acoustic features using Uniform Manifold Approximation and Projection (UMAP). The 2D UMAP projection (Figure S5) offers a qualitative view of local neighbourhoods in the feature space. In this space, a substantial overlap is observed between control (red) and VPA (blue) calls, indicating largely shared variance across the feature set, with only localised regions of higher group concentration. This pattern suggests limited global separation in the manifold; given that UMAP preserves local structure and depends on hyperparameters and random initialisation, these projections should be interpreted as qualitative rather than inferential. Quantitative analysis for condition effects was therefore assessed at the feature level using linear mixed-effects models, as seen in Section 3.2.2.

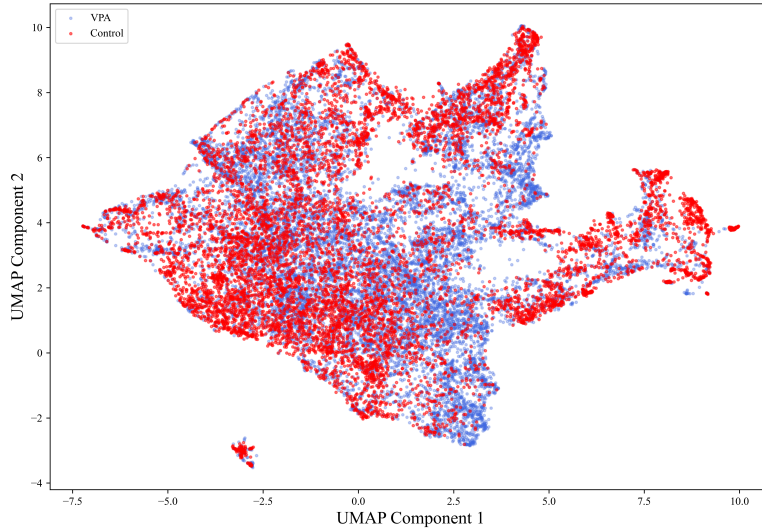


Figure S5: 2D UMAP of call-level acoustic features for control (red) and VPA (blue). UMAP was run on z-scored features (Euclidean metric)

S5. Multicollinearity Analysis

Before fitting the Linear Mixed Models, we assessed multicollinearity to avoid inflated variances and redundancy among predictors.

Variance Inflation Factor (VIF) values were calculated for all acoustic features to assess the degree of multicollinearity in the dataset. Features that exceeded the conventional threshold of 10 were flagged as potentially problematic. The analysis revealed significant multicollinearity among several frequency domain features, with F0 Standard Deviation and F0 Bandwidth exhibiting the highest VIF values, at 28.77 and 28.67, respectively. This indicates that these features share approximately 96% of their variance with other predictors in the model. Other features with elevated VIF values included Attack Magnitude (VIF = 8.27), RMS Standard Deviation (VIF = 7.97), RMS Mean (VIF = 7.49), F0 Mean (VIF = 5.48), and Spectral Centroid Mean (VIF = 4.65).

The pairwise correlation analysis revealed several highly correlated feature pairs ($|r| \geq 0.8$), especially within the frequency and energy domains, as illustrated in Figure S6.

Notable high correlations included F0 Standard Deviation and F0 Bandwidth ($r = 0.97$), Attack time and Duration call ($r = 0.91$), RMS Standard Deviation and Attack magnitude ($r = 0.92$), RMS Mean and Attack magnitude ($r = 0.85$), RMS Mean and RMS Standard Deviation ($r = 0.85$), and F0 Mean and Spectral Centroid Mean ($r = 0.82$).

To address multicollinearity while preserving discriminative power, a systematic feature selection approach

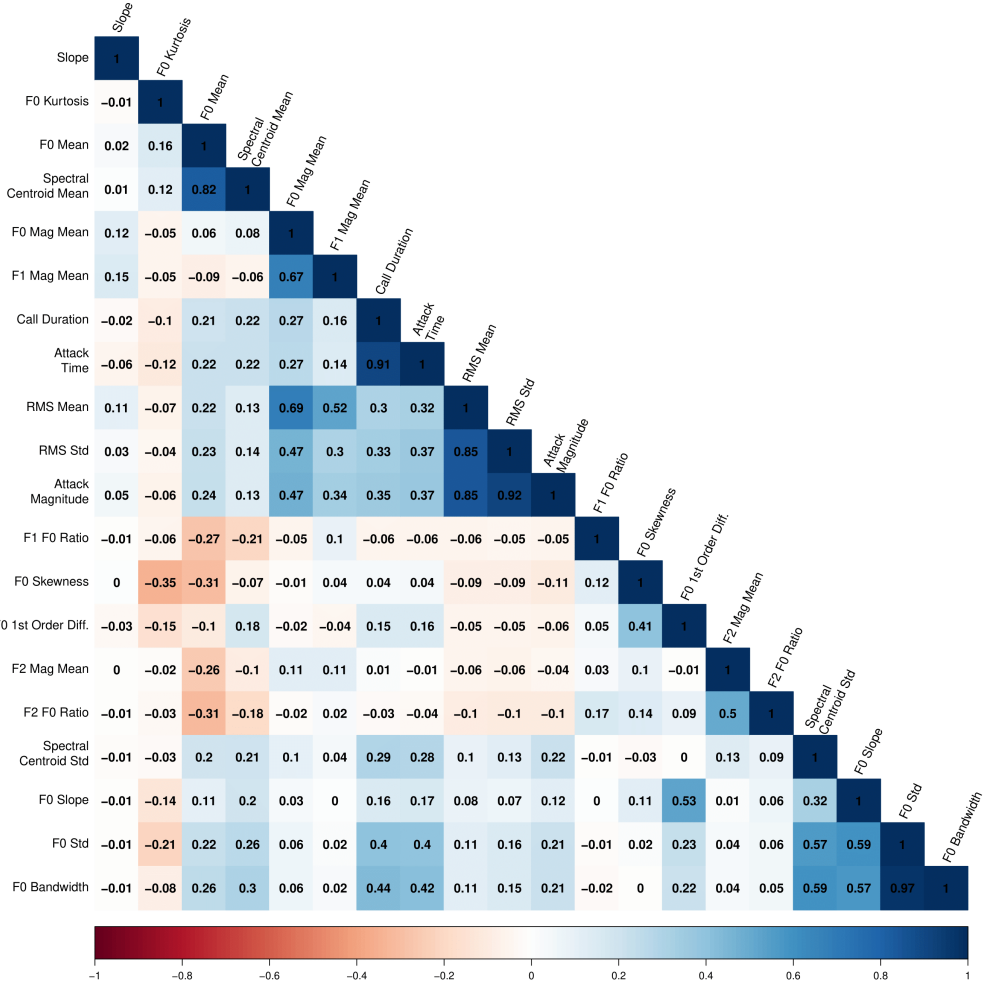


Figure S6: Correlation matrix of acoustic features computed using Pearson's correlation coefficients. Feature pairs exhibiting strong linear associations ($|r| \geq 0.8$) were identified to assess multicollinearity and inform subsequent feature selection.

was implemented.

For each pair of highly correlated features, discriminative power was quantified using Cohen's d effect sizes for group differences. From the highly correlated pairs, the following features were selected based on superior discriminative power and interpretability: Duration Call (in this case prioritising biological interpretability despite slightly lower discriminative power; Cohen's $d = 0.175$) over Attack time ($d = 0.208$), Spectral Centroid Mean ($d = 0.364$) over F0 Mean ($d = 0.271$), F0 Standard Deviation ($d = 0.331$) over F0 Bandwidth ($d = 0.282$), RMS Mean ($d = 0.364$) and Attack magnitude ($d = 0.385$) over RMS Std ($d = 0.316$).

The final feature set for the LMM analysis included 16 features: Duration Call, F0 Standard Deviation, F0 Skewness, F0 Kurtosis, F0 1st Order Difference, F0 Slope, F0 Magnitude Mean, F1 Magnitude Mean, F2 Magnitude Mean, F1-F0 Ratio, F2-F0 Ratio, Spectral Centroid Mean, Spectral Centroid Standard Deviation, RMS Mean, Envelope Slope, and Attack Magnitude. This feature selection ensured that the subsequent analyses were conducted with a robust set of predictors, covering the vocal acoustic space while maximising discriminatory power between experimental conditions.

S6. Feature analysis

S6.1 Linear Mixed Models Results Across the 20 Acoustic Features

This section reports the full results of the Linear Mixed Models (LMM) fitted on all 20 extracted acoustic features, analysed across six recording time bins and stratified by cluster and experimental condition (CTRL vs VPA). The models also included chick ID as a random intercept to account for repeated measures. Results are based on the 2-cluster solution identified via hierarchical clustering and are grouped by acoustic domain (temporal, energy, frequency).

Table S4 provides detailed statistics for all main effects and interactions, including χ^2 , FDR-corrected p -values, and partial η^2 effect sizes. The 16 features retained in the main analysis are discussed in the Results section 3.2.2; additional features are included here for completeness.

Feature	Cluster			Condition			Temporal Bin			Condition \times Cluster		
	χ^2	p	η^2	χ^2	p	η^2	χ^2	p	η^2	χ^2	p	η^2
Temporal Domain												
Call Duration	3846.09	< 0.001	0.997	629.82	< 0.001	0.981	413.08	< 0.001	0.954	617.35	< 0.001	0.990
Attack Time	3896.02	< 0.001	0.997	616.08	< 0.001	0.981	345.69	< 0.001	0.945	595.90	< 0.001	0.990
Slope	282.87	< 0.001	0.959	71.89	< 0.001	0.857	205.01	< 0.001	0.911	62.61	< 0.001	0.913
Energy Domain												
RMS Mean	14119.73	< 0.001	0.999	1013.94	< 0.001	0.988	2605.85	< 0.001	0.992	730.42	< 0.001	0.992
RMS Standard Deviation	9294.08	< 0.001	0.999	543.23	< 0.001	0.978	1769.53	< 0.001	0.989	388.98	< 0.001	0.985
Frequency Domain												
F0 Mean	1108.25	< 0.001	0.989	107.27	< 0.001	0.899	469.74	< 0.001	0.959	50.68	< 0.001	0.894
F0 Standard Deviation	3850.06	< 0.001	0.997	1013.91	< 0.001	0.988	463.79	< 0.001	0.959	927.37	< 0.001	0.994
F0 Skewness	31.15	0.002	0.722	21.64	0.042	0.643	105.29	< 0.001	0.840	11.34	0.078	0.654
F0 Kurtosis	260.25	< 0.001	0.956	54.72	< 0.001	0.820	123.76	< 0.001	0.861	27.72	< 0.001	0.822
F0 Bandwidth	3417.33	< 0.001	0.997	861.09	< 0.001	0.986	418.59	< 0.001	0.954	773.95	< 0.001	0.992
F0 1st Order Difference	921.62	< 0.001	0.987	184.11	< 0.001	0.939	290.95	< 0.001	0.936	170.88	< 0.001	0.966
F0 Slope	3467.01	< 0.001	0.997	766.67	< 0.001	0.985	988.87	< 0.001	0.980	677.26	< 0.001	0.991
F0 Mag Mean	5725.45	< 0.001	0.998	825.49	< 0.001	0.986	1584.43	< 0.001	0.988	678.42	< 0.001	0.991
F1 Mag Mean	3273.14	< 0.001	0.996	234.11	< 0.001	0.951	841.67	< 0.001	0.977	166.81	< 0.001	0.965
F2 Mag Mean	43.37	< 0.001	0.783	19.66	0.074	0.621	299.11	< 0.001	0.937	7.29	0.295	0.549
F1-F0 Ratio	63.27	< 0.001	0.841	26.08	0.010	0.685	53.13	< 0.001	0.727	14.93	0.021	0.713
F2-F0 Ratio	47.68	< 0.001	0.799	16.41	0.173	0.578	122.86	< 0.001	0.860	2.93	0.818	0.328
Spectral Centroid Mean	1605.07	< 0.001	0.993	166.94	< 0.001	0.933	267.72	< 0.001	0.930	99.57	< 0.001	0.943
Spectral Centroid Std	866.20	< 0.001	0.986	251.38	< 0.001	0.954	324.61	< 0.001	0.942	105.14	< 0.001	0.946
Attack Magnitude	10029.14	< 0.001	0.999	688.62	< 0.001	0.983	1542.17	< 0.001	0.987	556.52	< 0.001	0.989

Table S4: Linear Mixed Models results for acoustic features across temporal, energy, and frequency domains. Effect sizes (η^2) and statistical significance are reported for main effects and interactions following FDR correction ($\alpha = 0.05$).

S6.2 Complete Statistical Results: Additional Significant Features

This section reports detailed results and plots of features that showed significant effects but were excluded from the main text due to lower effect sizes or high correlations with other features. Although omitted for brevity, these results support the robustness of the main findings.

S6.2.1 Temporal Domain Features We found similar patterns for Attack Time and Envelope Slope, with the minimum adequate model including the interaction between Condition, Cluster membership, and Time bin (see Supplementary Table S4). For Attack Time, the analysis revealed a significant three-way interaction ($\chi^2 = 44.40$, $p < 0.001$, $\eta^2 = 0.649$) and a condition \times cluster interaction ($\chi^2 = 595.90$, $p < 0.001$, $\eta^2 = 0.990$). This feature was excluded from the main analysis due to high correlation with Call Duration ($r = 0.91$). As expected, the pattern of results mirrors those observed for Call Duration: while cluster 0 calls showed no differences between conditions, cluster 1 calls exhibited significantly longer attack times in control compared to VPA chicks (post-hoc: $p < 0.001$). This difference remained stable across the recording session (see Figure S7A).

For Envelope Slope, the analysis revealed a significant three-way interaction ($\chi^2 = 62.65$, $p < 0.001$, $\eta^2 = 0.723$) and a strong condition \times cluster interaction ($\chi^2 = 557.02$, $p < 0.001$, $\eta^2 = 0.984$). Cluster 1 calls demonstrated condition-specific temporal dynamics that varied across the recording session (see Figure S7B).

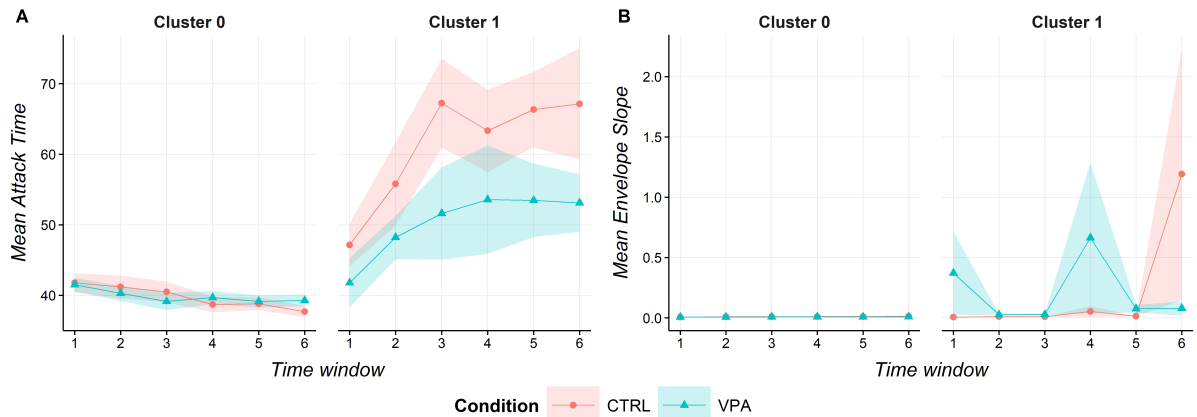


Figure S7: Temporal-domain features across time bins by condition and cluster. (A) Attack Time, (B) Envelope Slope. Mean \pm SEM

S6.2.2 Energy Domain Features For RMS Standard Deviation, the minimum adequate model included the interaction between Condition, Cluster membership, and Time bin (see Supplementary Table S4). The analysis revealed significant main effects for Cluster ($\chi^2 = 9294.08$, $p < 0.001$, $\eta^2 = 0.999$), Condition ($\chi^2 = 543.23$, $p < 0.001$, $\eta^2 = 0.978$), and Temporal Bin ($\chi^2 = 1769.53$, $p < 0.001$, $\eta^2 = 0.989$), as well as a strong condition \times cluster interaction ($\chi^2 = 388.98$, $p < 0.001$, $\eta^2 = 0.985$). This feature was excluded from the main text due to high correlation with RMS Mean ($r = 0.85$), though it displays a complementary pattern. Cluster 1 calls showed higher energy variability in VPA-exposed chicks compared to controls (post-hoc: $p < 0.001$), while cluster 0 calls exhibited reduced energy variability under VPA conditions (post-hoc: $p = 0.015$), albeit with a smaller effect magnitude. These findings support that VPA exposure affects both the average energy level and its variability in a call-type-specific manner (Figure S8).

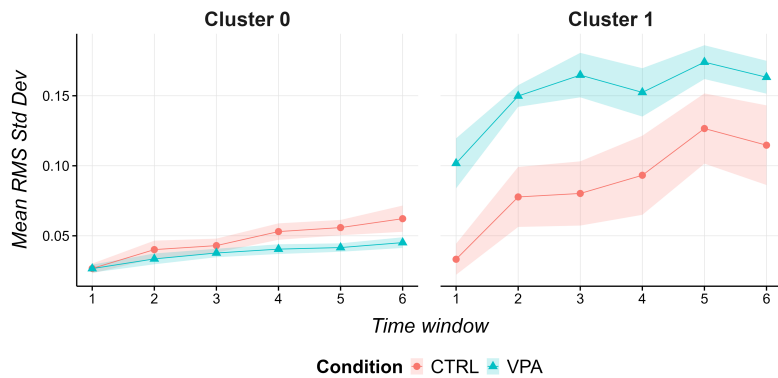


Figure S8: RMS Standard Deviation across 6 time bins, plotted by condition and cluster (2-cluster solution). Mean \pm SEM.

S6.2.3 Frequency Domain Features We found similar patterns for features related to fundamental frequency features (F0 Mean, F0 Skewness, F0 Magnitude Mean), with the minimum adequate model including the interaction between Condition, Cluster membership, and Time bin (see Supplementary Table S4).

For F0 Mean, the analysis showed significant main effects for Cluster ($\chi^2 = 1108.25$, $p < 0.001$, $\eta^2 = 0.989$) and Condition ($\chi^2 = 107.27$, $p < 0.001$, $\eta^2 = 0.899$), with a modest three-way interaction ($\chi^2 = 11.48$, $p = 0.043$, $\eta^2 = 0.324$). This feature was excluded from the main analysis due to high correlation with Spectral Centroid Mean ($r = 0.82$). While post-hoc comparisons did not reveal significant condition differences within clusters (cluster 0: $p = 0.156$; cluster 1: $p = 0.717$), temporal dynamics suggested subtle condition-dependent variations in fundamental frequency that varied during the recording session (Figure S9A). For F0 Magnitude Mean, the analysis showed a very strong three-way interaction ($\chi^2 = 347.04$, $p < 0.001$, $\eta^2 = 0.935$). This feature exhibited a striking temporal inversion pattern, particularly for cluster 1 calls. VPA-exposed chicks initially showed higher F0 magnitude values, but these progressively declined over the recording session. In contrast, control chicks demonstrated the opposite temporal trajectory (post-hoc cluster 1: $p < 0.001$). Cluster 0 calls showed no significant condition differences (post-hoc: $p = 0.908$) (see Figure S9B). For F0 Skewness, the analysis revealed a significant three-way interaction ($\chi^2 = 11.29$, $p = 0.046$, $\eta^2 = 0.320$). However, the effect sizes were considerably smaller than those observed for other frequency variability features reported in the main text (F0 Standard Deviation, F0 Kurtosis). Post-hoc comparisons showed no significant differences within clusters (cluster 0: $p = 0.970$; cluster 1: $p = 0.959$), confirming that while F0 Skewness differed between call types and showed subtle condition effects, these were less pronounced than other pitch distribution measures (Figure S9C).

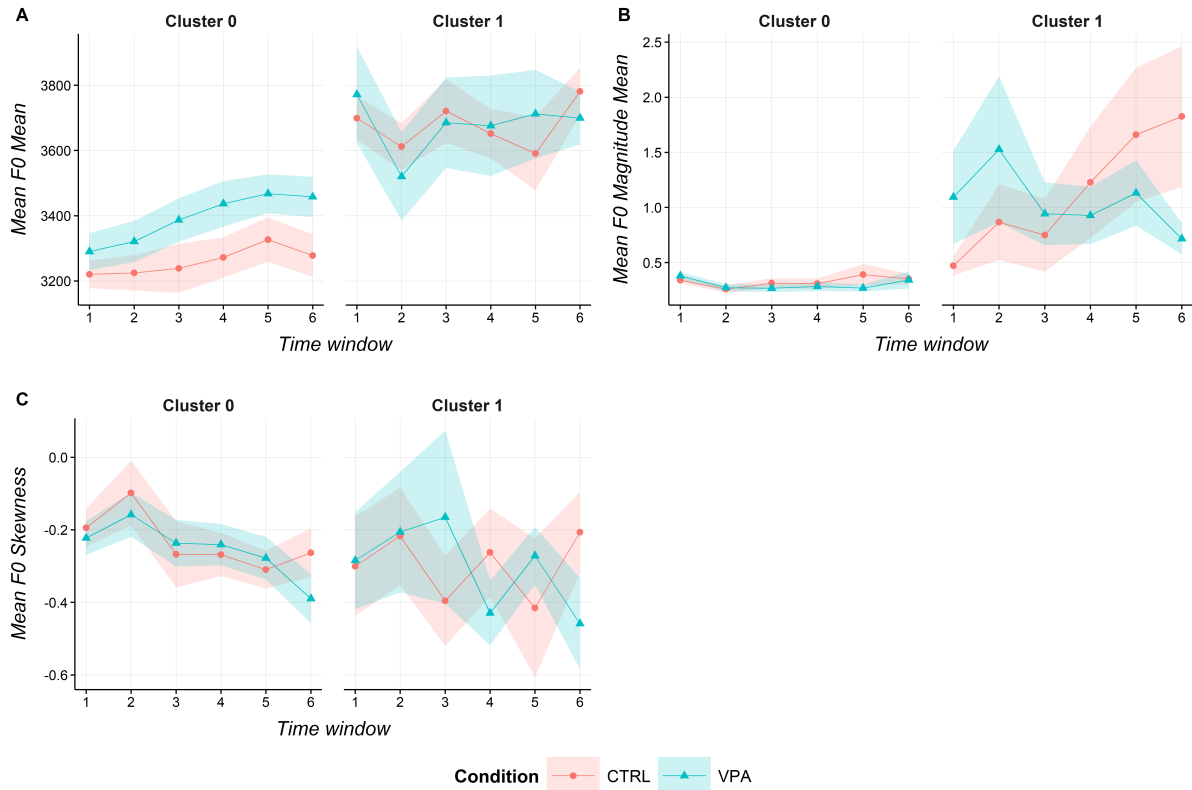


Figure S9: Frequency-domain features across 6 time bins by condition and cluster. (A) F0 Mean, (B) F0 Magnitude Mean, (C) F0 Skewness. Mean \pm SEM

Harmonic-related features revealed distinctive patterns based on their acoustic properties. We examined both magnitude features (F1 Magnitude Mean, F2 Magnitude Mean) and ratio features (F1/F0 Ratio, F2/F0 Ratio).

For F1 Magnitude Mean, the minimum adequate model included the interaction between Condition, Cluster

membership, and Time bin (see Supplementary Table S4), with a strong three-way interaction ($\chi^2 = 164.39$, $p < 0.001$, $\eta^2 = 0.873$). Similarly to F0 Magnitude Mean, this feature showed temporal inversion patterns. VPA-treated chicks showed a progressive reduction in first formant magnitude across later time bins, while control values increased over time. However, post-hoc comparisons revealed no significant condition differences within either cluster (cluster 0: $p = 0.743$; cluster 1: $p = 0.811$), likely due to high within-group variability and the complex temporal dynamics (Figure S10A).

For F1/F0 Ratio, the minimum adequate model included two-way interactions but not the three-way interaction (see Supplementary Table S4; $\chi^2 = 4.89$, $p = 0.430$). The analysis revealed significant main effects of Cluster ($\chi^2 = 63.27$, $p < 0.001$, $\eta^2 = 0.841$), Condition ($\chi^2 = 26.08$, $p = 0.010$, $\eta^2 = 0.685$) and Temporal Bin ($\chi^2 = 53.13$, $p < 0.001$, $\eta^2 = 0.727$), together with a weak but significant condition \times cluster interaction ($\chi^2 = 14.93$, $p = 0.021$, $\eta^2 = 0.713$). The pattern differed markedly from magnitude features. Cluster 0 calls showed a small but consistent divergence between conditions across time bins (post-hoc: $p = 0.033$), with VPA exposure associated with slightly elevated F1/F0 ratios. In contrast, cluster 1 calls displayed large within-group variability and overlapping trends between conditions, particularly after 120 seconds (post-hoc: $p = 0.548$). These stable temporal dynamics, without dramatic inversions, suggest that VPA exposure affects the spectral balance between F1 and F0 through mechanisms distinct from those affecting absolute formant magnitudes (Figure S10B).

For F2 Magnitude Mean, the minimum adequate model included only two-way interactions (see Supplementary Table S4), as the three-way interaction was not significant ($\chi^2 = 1.24$, $p = 0.941$). The analysis showed a significant main effect of Cluster ($\chi^2 = 43.37$, $p < 0.001$, $\eta^2 = 0.783$) and a condition \times cluster interaction ($\chi^2 = 6.08$, $p = 0.014$, $\eta^2 = 0.243$). Unlike F0 and F1 magnitude features, F2 Magnitude Mean showed more stable patterns across time bins. Post-hoc comparisons suggested subtle differences between conditions (cluster 0: $p = 0.067$; cluster 1: $p = 0.443$), but the effects were less consistent and of smaller magnitude compared to the lower formants (Figure S10C).

Finally, for F2/F0 Ratio, the minimum adequate model included only main effects (see Supplementary Table S4), as neither the three-way interaction ($\chi^2 = 1.21$, $p = 0.944$) nor the two-way interactions ($\chi^2 = 10.60$, $p = 0.477$) were significant. The analysis showed significant main effects of Cluster ($\chi^2 = 47.68$, $p < 0.001$, $\eta^2 = 0.799$) and Condition ($\chi^2 = 5.93$, $p = 0.015$, $\eta^2 = 0.426$). This suggests that VPA exposure uniformly affects the ratio between the second formant and fundamental frequency, regardless of call type or temporal dynamics (Figure S10D).

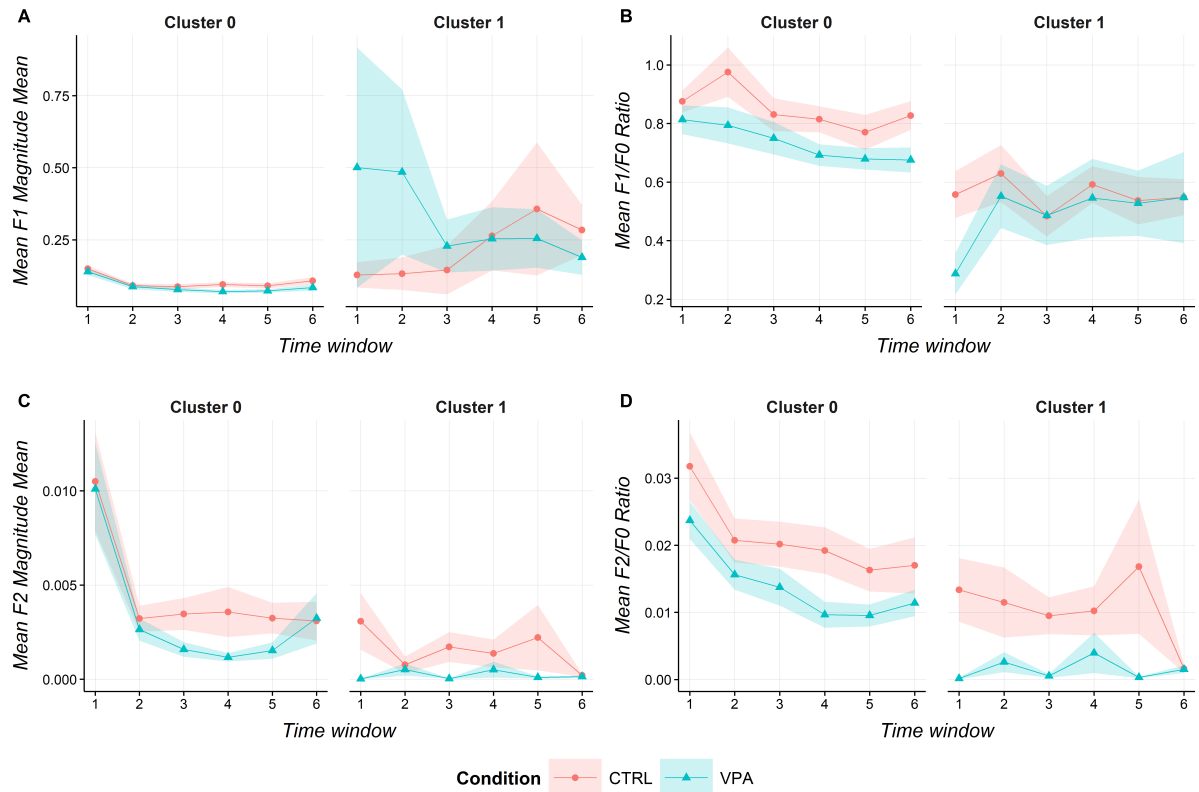


Figure S10: Harmonic-related features across 6 time bins by condition and cluster. (A) $F1$ Magnitude Mean, (B) $F1-F0$ Ratio, (C) $F2$ Magnitude Mean, (D) $F2-F0$ Ratio. Mean \pm SEM.

S6.3 Post Hoc Tukey Statistical Results

To further characterise the significant *condition* \times *cluster* interactions identified in the LMM analysis, we conducted post-hoc Tukey-adjusted pairwise comparisons. Table S5 presents all acoustic features that showed significant differences between VPA-exposed and control groups within specific clusters, organised by acoustic domain. The results reveal that Cluster 1 calls exhibited substantially more condition-sensitive features across all acoustic domains compared to Cluster 0, indicating differential vulnerability to prenatal VPA exposure between call types.

Cluster 0	Cluster 1
Temporal Domain	
	<i>Call Duration</i> CTRL > VPA ($p < 0.001$)
	<i>Attack Time</i> CTRL > VPA ($p < 0.001$)
Energy Domain	
	<i>RMS Mean</i> CTRL < VPA ($p = 0.001$)
	<i>RMS Standard Deviation</i> CTRL < VPA ($p < 0.001$)
Frequency Domain	
<i>Attack Magnitude</i> CTRL > VPA ($p = 0.031$)	<i>Attack Magnitude</i> CTRL < VPA ($p < 0.001$)
<i>Spectral Centroid Standard Deviation</i> CTRL > VPA ($p = 0.005$)	<i>Spectral Centroid Standard Deviation</i> CTRL > VPA ($p < 0.001$)
<i>F0 Kurtosis</i> CTRL < VPA ($p < 0.001$)	<i>F0 Kurtosis</i> CTRL < VPA ($p < 0.001$)
	<i>F0 Standard Deviation</i> CTRL > VPA ($p < 0.001$)
	<i>F0 Bandwidth</i> CTRL < VPA ($p < 0.001$)
	<i>F0 1st Order Difference</i> CTRL > VPA ($p < 0.001$)
	<i>F0 Slope</i> CTRL > VPA ($p < 0.001$)
	<i>F0 Magnitude Mean</i> CTRL > VPA ($p < 0.001$)
<i>F1/F0 Ratio</i> CTRL > VPA ($p = 0.034$)	

Table S5: Post-hoc Tukey test results for significant *Condition* \times *Cluster* interactions. The table reports acoustic features significantly different between the VPA and CTRL groups within either cluster 0 or 1, following FDR correction. CTRL > VPA: control group had higher values than VPA-exposed; CTRL < VPA: control group had lower values.

S7. Average calls and comparison with literature

The following section presents the mean values for acoustic features across clusters identified in this study for both the development dataset and the experimental datasets (control and VPA groups).

Feature	Development data		control group		VPA group	
	Cluster 0 (n=3460)	Cluster 1 (n=2173)	Cluster 0 (n=7661)	Cluster 1 (n=1367)	Cluster 0 (n=13632)	Cluster 1 (n=889)
Temporal Domain						
Duration (s)	0.148 \pm 0.049	0.364 \pm 0.074	0.115 \pm 0.033	0.186 \pm 0.058	0.117 \pm 0.032	0.145 \pm 0.045
Attack Time	27.382 \pm 15.16	66.243 \pm 13.914	39.47 \pm 14.81	73.64 \pm 29.04	40.05 \pm 14.87	53.40 \pm 21.55
Energy Domain						
RMS Mean	0.028 \pm 0.022	0.147 \pm 0.051	0.097 \pm 0.090	0.383 \pm 0.271	0.070 \pm 0.052	0.420 \pm 0.158
RMS Std	0.017 \pm 0.019	0.140 \pm 0.047	0.051 \pm 0.048	0.155 \pm 0.102	0.041 \pm 0.030	0.177 \pm 0.063
Attack Magnitude	0.151 \pm 0.138	0.975 \pm 0.219	0.382 \pm 0.294	1.023 \pm 0.576	0.290 \pm 0.196	1.181 \pm 0.325
Frequency Domain						
F0 Mean (Hz)	3036 \pm 457	3344 \pm 266	3272 \pm 426	3782 \pm 305	3471 \pm 496	3582 \pm 347
F0 Std (Hz)	293 \pm 141	351 \pm 132	173 \pm 105	404 \pm 200	163 \pm 115	190 \pm 131
F0 Skewness	0.054 \pm 0.651	0.393 \pm 0.656	-0.29 \pm 0.82	-0.36 \pm 0.58	-0.34 \pm 0.95	-0.44 \pm 0.66
F0 Kurtosis	-0.795 \pm 0.790	-0.428 \pm 0.828	-0.58 \pm 1.14	-1.10 \pm 0.88	-0.25 \pm 1.31	-0.68 \pm 1.16
F0 Bandwidth (Hz)	893 \pm 399	1218 \pm 402	502 \pm 282	1073 \pm 466	488 \pm 314	551 \pm 343
F0 1st Order Diff	46.405 \pm 63.016	4.613 \pm 17.251	-2.88 \pm 51.79	39.90 \pm 68.67	3.93 \pm 52.11	14.66 \pm 41.14
F0 Slope	8022 \pm 6457	11782 \pm 7538	3408 \pm 3905	11486 \pm 11434	3174 \pm 4359	4681 \pm 4631
F0 Magnitude Mean	0.231 \pm 0.493	0.658 \pm 0.518	0.329 \pm 0.562	2.508 \pm 2.885	0.288 \pm 0.418	1.673 \pm 2.194
F1 Magnitude Mean	0.028 \pm 0.054	0.010 \pm 0.018	0.100 \pm 0.108	0.467 \pm 0.829	0.077 \pm 0.089	0.487 \pm 0.836
F2 Magnitude Mean	0.000 \pm 0.000	0.000 \pm 0.000	0.0037 \pm 0.019	0.00052 \pm 0.003	0.0022 \pm 0.015	0.00017 \pm 0.001
F1/F0 Ratio	0.273 \pm 0.408	0.061 \pm 0.098	0.828 \pm 1.333	0.545 \pm 0.486	0.669 \pm 0.751	0.610 \pm 0.569
F2/F0 Ratio	0.000 \pm 0.002	0.000 \pm 0.000	0.0187 \pm 0.074	0.0043 \pm 0.018	0.0109 \pm 0.051	0.0012 \pm 0.010
Spectral Centroid Mean (Hz)	5565 \pm 1121	5869 \pm 800	5946 \pm 1188	7374 \pm 925	6610 \pm 1252	6723 \pm 1038
Spectral Centroid Std (Hz)	1045 \pm 407	1196 \pm 392	908 \pm 518	1370 \pm 537	757 \pm 452	798 \pm 452
Envelope Slope	0.007 \pm 0.006	0.015 \pm 0.004	0.0110 \pm 0.027	0.113 \pm 1.348	0.0080 \pm 0.009	0.112 \pm 0.956

Table S6: Mean \pm standard deviation of acoustic features for the identified clusters across development and experimental datasets (control and VPA groups).

The following results are presented in comparison to the findings of the existing literature. Table S7 compares our computational framework results with the classifications reported by Marx et al. [18], highlighting quantitative differences.

Dataset	Cluster	Duration (ms)	Energy (RMS)	F0 Mean (kHz)	F0 Frequency Modulation	Literature Comparison (Marx et al.)
Development	Cluster 0	148 ± 49	0.028 ± 0.022	3.04 ± 0.46	Ascending modulation(F0 1st diff +46.4 Hz) ; Onset low and high peak(F0 slope +8.0 kHz/s) ; (Upward trend) F0 bandwidth 893 Hz.	Alignment with pleasure calls. Duration: 148ms vs Marx 23–90ms. Energy: 0.028 vs Marx 0.001–0.02. F0: 3.0kHz vs Marx 2.5–5.5kHz. Ascending matches Marx's pleasure calls identified pattern.
	Cluster 1	364 ± 74	0.147 ± 0.051	3.34 ± 0.27	Stable/Flat modulation (F0 1st diff +4.6 Hz) ; Minimal frequency change (F0 slope +11.8 kHz/s); High bandwidth suggests complexity (F0 bandwidth 1218 Hz).	Alignment with contact calls. Duration: 364ms vs Marx 100–250ms. Energy: 0.147 vs Marx 0.02–2 . F0: 3.3kHz vs Marx 2–6.5kHz . Extended duration, stable F0 = contact function.
Control Group	Cluster 0	115 ± 33	0.097 ± 0.090	3.27 ± 0.43	Slightly Descending modulation (F0 1st diff -2.9 Hz) ; Minimal downward trend (F0 slope +3.4 kHz/s) ; Low bandwidth modulation (F0 bandwidth 502 Hz)	Partially match short peep. Duration: 115ms vs Marx 40–100ms . Energy: 0.097 vs Marx 0.004–0.01. F0: 3.3kHz vs Marx 3–5kHz . Descending modulation matches short peep pattern.
	Cluster 1	186 ± 58	0.383 ± 0.271	3.78 ± 0.31	Moderately Ascending frequency(F0 1st diff +39.9 Hz; F0 slope +11.5 kHz/s); High bandwidth = complex (F0 bandwidth 1073 Hz).	Match contact call. Duration: 186ms vs Marx 100–250ms . Energy: 0.383 vs Marx 0.02–2 . F0: 3.8kHz vs Marx 2–6.5kHz . Ascending frequency modulation consistent with contact function.
VPA Group	Cluster 0	117 ± 32	0.070 ± 0.052	3.47 ± 0.50	Weakly Ascending modulation(F0 1st diff +3.9 Hz; Flattened frequency contour (F0 slope +3.2 kHz/s) ; F0 bandwidth 488 Hz	Partial matching short peep. Duration: 117ms vs Marx 40–100ms. Energy: 0.070 vs Marx 0.004–0.01. F0: 3.5kHz vs Marx 3–5kHz . Atypical ascending vs Marx descending pattern.
	Cluster 1	145 ± 45	0.420 ± 0.158	3.58 ± 0.35	Weakly Ascending modulation(F0 1st diff +14.7 Hz; F0 slope +4.7 kHz/s; Low bandwidth = impaired complexity (F0 bandwidth 551 Hz).	Partial matching contact call. Duration: 145ms vs Marx 100–250ms . Energy: 0.420 vs Marx 0.02–2 . F0: 3.6kHz vs Marx 2–6.5kHz . Atypical ascending vs Marx descending; reduced complexity.

Table S7: Comparison of identified clusters in the development and experimental datasets with call types described from Marx et al. [18]